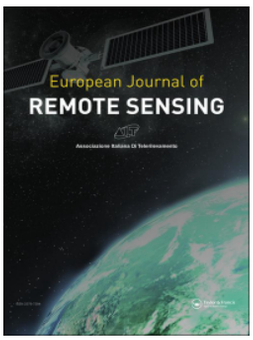

European Journal of Remote Sensing

ISSN: (Print) (Online) Journal homepage: https://www.tandfonline.com/loi/tejr20

Near-real time deforestation detection in the Brazilian Amazon with Sentinel-1 and neural networks

Claudia Arantes Silva, Giorgia Guerrisi, Fabio Del Frate & Edson Eyji Sano

To cite this article: Claudia Arantes Silva, Giorgia Guerrisi, Fabio Del Frate & Edson Eyji Sano (2022) Near-real time deforestation detection in the Brazilian Amazon with Sentinel-1 and neural networks, European Journal of Remote Sensing, 55:1, 129-149, DOI: 10.1080/22797254.2021.2025154

To link to this article: https://doi.org/10.1080/22797254.2021.2025154

Published online: 27 Jan 2022.

EUROPEAN JOURNAL OF REMOTE SENSING
2022, VOL. 55, NO. 1, 129–149
https://doi.org/10.1080/22797254.2021.2025154

Taylor & Francis
Taylor & Francis Group

Near-real time deforestation detection in the Brazilian Amazon with Sentinel-1 and neural networks

Claudia Arantes Silva[a], Giorgia Guerrisi[b], Fabio Del Frate[b] and Edson Eyji Sano[c]

[a]Institute of Geosciences, Applied Geosciences and Geodynamics Program, Universidade de Brasília, Brasília, Brazil; [b]EMBRAPA (Brazilian Agricultural Research Corporation),Brasilla, Brazil; [c]Civil Engineering and Computer Science Engineering Department, University of Rome "Tor Vergata", Rome, Italy

ABSTRACT

Optical-based near-real time deforestation alert systems in the Brazilian Amazon are ineffective in the rainy season. This study identify clear-cut deforested areas through Neural Network (NN) algorithm based on C-band, VV- and VH-polarized, Sentinel-1 images. Statistical parameters of backscatter coefficients (mean, standard deviation, and the difference between maximum and minimum values – MMD) were computed from 30 Sentinel-1 images, from 2019, used as input parameters of the NN classifier. The samples were manually selected, including forested and deforested areas. After deforestation, mean backscatter signals decreased on the average of 2 dB for VV and 2.3 dB for VH from May to September–October. A Multi-Layer Perceptron (MLP) network was used for detecting near-real time forest disturbances larger than 2 ha. Case studies were performed for both polarizations considered the following input sets to the MLP: mean; mean and standard deviation; mean and MMD; and mean, standard deviation, and MMD. For the 2019 dataset, the latter showed the best performance of the NN algorithm with accuracy and F1 score of 99%. Automatic extraction using 2018 Sentinel-1 images reached accuracy and F1 score of 89% with the MapBiomas reference data and accuracy of 81% and F1 score of 79% with the PRODES reference data.

ARTICLE HISTORY
Received 15 July 2021
Revised 30 October 2021
Accepted 30 December 2021

KEYWORDS
Amazon forest; neural network; MLP; multi-layer perceptron; time series analysis; change detection; near-real time deforestation detection

Introduction

The Brazilian Amazon covers an area of approximately 5.2 million km^2, about 60% of the Brazilian territory, encompassing the following states: Acre (AC), Amapá (AP), Amazonas (AM), Mato Grosso (MT), Pará (PA), Rondônia (RO), Roraima (RR), Tocantins (TO), and part of Maranhão (MA; Figure 1). Satellite-based monitoring of such a large territory is a complex task because of its continental size and long rainy seasons. Forest disturbance in the Brazilian Amazon by human occupation is mostly concentrated in a large region named deforestation arch. The arch has about 1.7 million km^2 (33% of the Brazilian Amazon), extends from northeast of Maranhão State to southeast of Acre State, and concentrates most of the monitoring efforts conducted by the Brazilian environmental organizations (Cochrane, 2003; Davidson et al., 2012; Farias et al., 2018; D. Nepstad et al., 2001; Souza et al., 2020; Yanai et al., 2017).

Clear-cut deforestation larger than 200 hectares was commonly observed in the region between 2000 and 2018 (Davis et al., 2020). In the last five years (2016–2020), the Brazilian Amazon has lost about 43,300 km^2 of forest cover. Deforestation, which is frequently associated with fire occurrences and illegal selective logging (Silva Júnior et al., 2018; Van Marle et al., 2017), exceeded 10,000 km^2 in 2019 and 10,800 km^2 in 2020. The Brazilian Amazon has also been degraded by intensive selective logging activities, causing a significant loss of forest diversity (Bezerra et al., 2021; Matricardi et al., 2020). Silva et al. (2021) recently addressed the dynamics of occupation and greenhouse gas emissions in this region. Pará is the state presenting the highest levels of deforestation since 2006, mostly driven by the rural settlement, beef production, crop plantation, and large reservoirs of hydropower plants (D. C. Nepstad et al., 1999; Farias et al., 2018; Kastens et al., 2017; Yanai et al., 2020).

The National Institute for Space Research (INPE) is the Brazilian institution responsible for monitoring annual deforestation in the Brazilian Amazon through the Project of the Deforestation Monitoring by Satellite (PRODES). The program relies on optical sensors onboard the Landsat 8, Sentinel-2, and China–Brazil Earth Resources Satellite (CBERS-4 and CBERS-4A) satellites. In this project, deforestation is defined as the conversion of primary forest into clear-cut areas (Diniz et al., 2015; Terrabrasilis – Geographic Data Platform, n. d.). Reports and deforestation data about the Brazilian Amazon can also be obtained from the Brazilian Annual Land Use and Land Cover Mapping Project (MapBiomas initiative). It is a non-governmental organization that generates annual land use and land cover (LULC) time series of the entire country through the Landsat satellite data processing and analysis in the Google Earth Engine platform (Davis et al., 2020; Mapbiomas Brasil, n.d.).

CONTACT Claudia Arantes Silva silvaclaudia.geo@gmail.com Instituto de Geociências (Ig), Universidade de Brasília, Brasília, Brazil

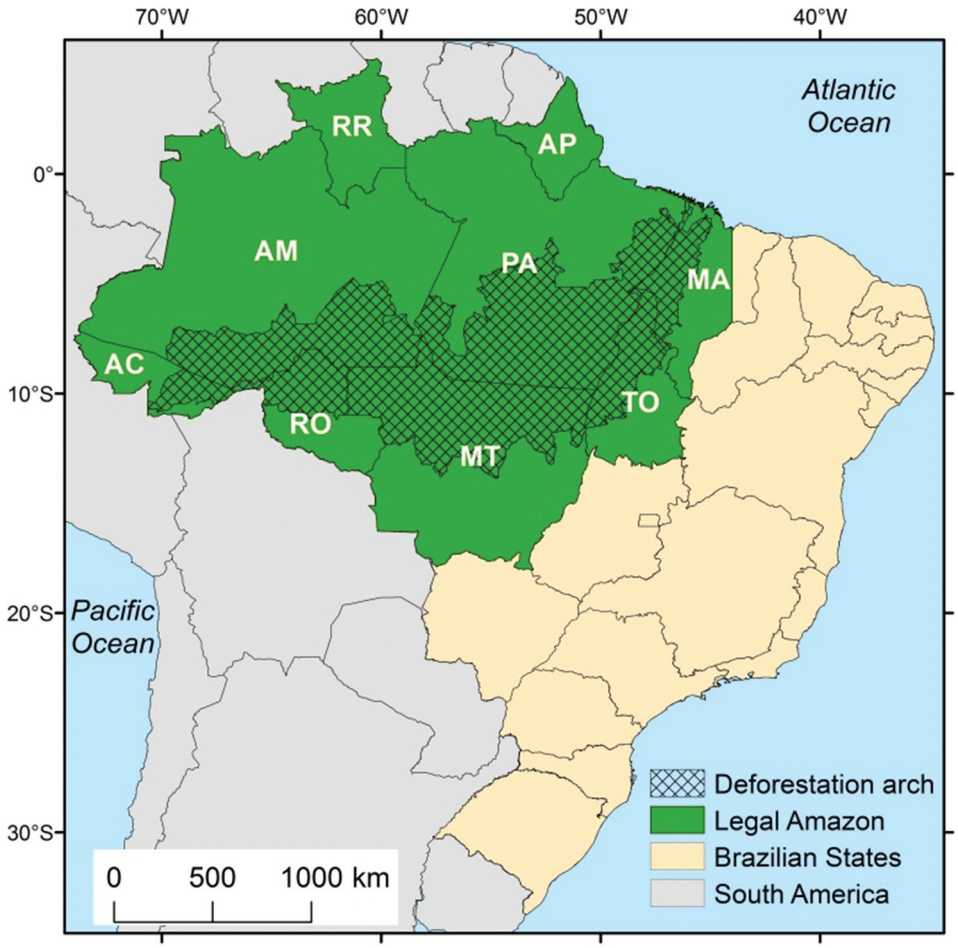

Figure 1. Location of the Brazilian Legal Amazon and the deforestation arch in Brazil. State identification: AC = Acre; AM = Amazonas; AP = Amapá; MA = Maranhão; MT = Mato Grosso; PA = Pará; RO = Rondônia; RR = Roraima; and TO = Tocantins.

During the rainy season, when the forest monitoring based on optical satellites is impaired, the Management and Operational Center for the Amazon Protection System (Censipam), from the Ministry of Defense, is the organization responsible for processing the X-band, synthetic aperture radar (SAR) images over critical areas. Regrettably, the reports issued by the institution are used basically for environmental law enforcement procedures. Figure 2 shows the deforestation process and weather conditions throughout the year in the Brazilian Amazon.

Currently, in terms of Brazilian satellites, the Brazilian Amazon is imaged by the joint Brazil–China, CBERS-4A optical satellite along with the Amazonia-1 satellite. The latter carries a wide-view optical imager with three visible (VIS) bands and one near-infrared (NIR) band with a swath of 850 km and 60 m of spatial resolution. The Ministry of Defense and INPE are currently conducting the zero-phase analysis of the national SAR mission. The integration of optical and SAR imageries can improve forest monitoring in tropical regions. Reiche et al. (2015) fused Landsat normalized difference vegetation index (NDVI) and L-band ALOS PALSAR backscatter time series in the Viti Levu Island, Fiji. They found a strong correlation between the backscatter multi-temporal HV/HH ratio and NDVI, while the accuracy using only NDVI decreased significantly.

Monitoring the Brazilian rainforest through remote sensing claims for some level of automation because of its large territorial extent. Neural networks (NNs) are one of the most advanced technological frontiers to increase the automation level in satellite image processing. A NN is a massively parallel distributed processor made up of simple processing units using cumulative empirical knowledge (Haykin, 2009). It has been successfully applied in different cases. Del Frate and Wang (2001) analysed the C- and L-band backscatter coefficients for retrieving sunflower biomass using NN algorithm to perform the inversion modelling. NN has been also applied to map the evolution of human settlements and urban land using C-band SAR images (Del Frate et al., 2008), to characterize the seismic source of an earthquake and its geometric parameters (Stramondo et al., 2011), to classify different crops by multi-polarized and multi-temporal backscattering coefficients (Del Frate et al., 2003), to detect land cover changes in urban areas

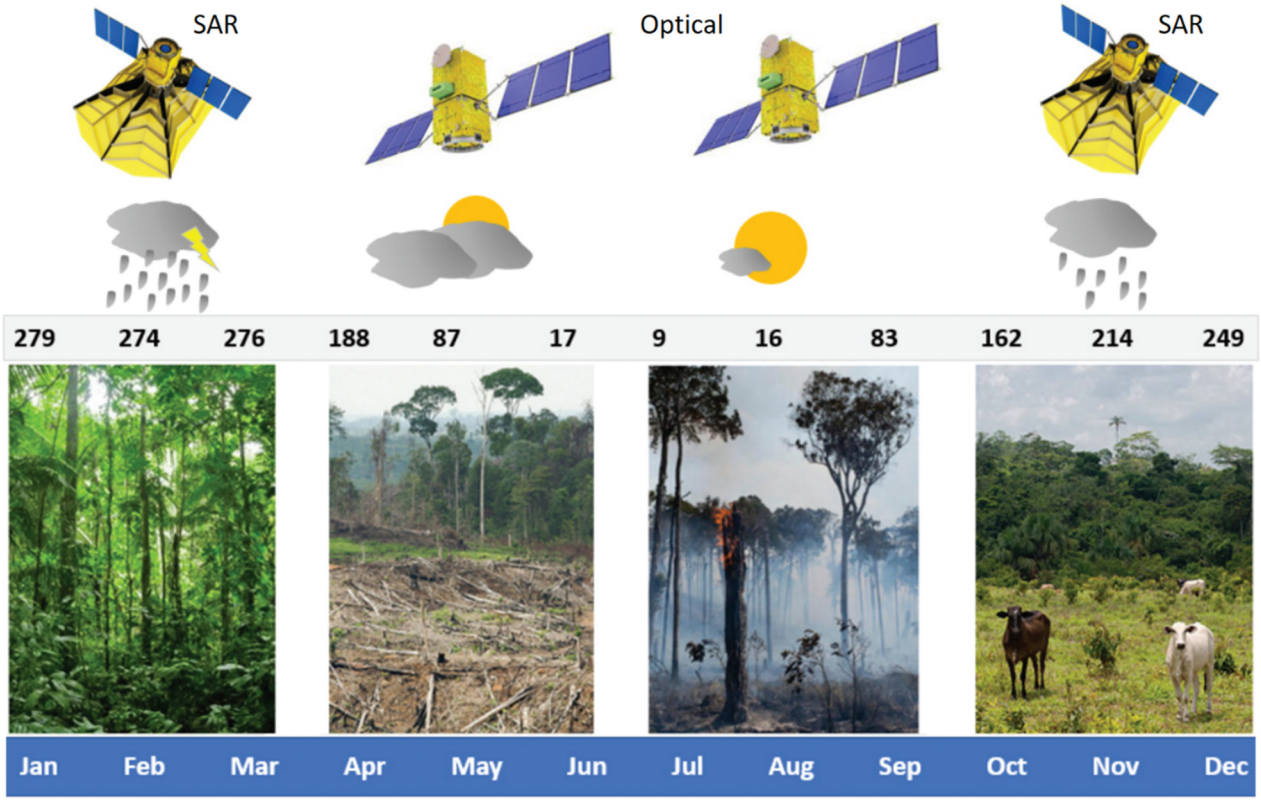

Figure 2. Deforestation process and weather conditions commonly found in the Brazilian Amazon over the year. The numbers above the images correspond to the monthly average precipitation (mm) for the southwest of Pará State from the period 1999–2020.

using X-band SAR images (Pratola et al., 2013), and to detect vegetation burnt areas to monitor regrowth of maquis vegetation with X-band data (Laurin et al., 2018).

Del Frate and Solimini (2004) proposed a NN algorithm to estimate soil moisture, leaf area index (LAI), and biomass in wheat fields. The algorithm was tested with experimental data collected at X-, C-, and S-bands. The model was based on the radiative transfer theory and a combination of scattering contributions. These authors obtained good results of moisture retrieval over bare soil and moderate results under vegetation cover. Even though the saturation effects reduced the absolute accuracy, the algorithm could reproduce the biomass trend with a reasonable agreement. Laurin et al. (2013) used the NN classifier to map areas of tropical forests in West Africa. In this study, the authors applied Landsat, ALOS AVNIR-2, and ALOS PALSAR data. The classification results were evaluated using optical data alone, SAR data alone, Landsat and PALSAR, AVNIR-2 and PALSAR, and a combination of three sensors. The integration of the three sensors reached the best results.

Few works have been conducted using machine learning algorithms or SAR images to detect deforestation in the Amazon rainforest. Bem et al. (2020) proposed a method based on convolutional neural networks (CNNs) applied to Landsat optical images from the Brazilian Amazon. They investigated different CNN architectures to predict annual changes in vegetation cover, comparing the results with two other machine learning algorithms, the Random Forest and the Multi-Layer Perceptron (MLP). They obtained good results employing CNNs, with the F1 score of 94–95%. However, CNNs are not widely accessible since they require a large number of samples and specific hardware for training, unlike other machine learning algorithms.

Doblas et al. (2020) suggested a procedure based on Sentinel-1 data, maximum likelihood classification (MLC), and adaptive thresholding (AT) for deforestation detection. They used SAR images acquired over 4 years (from November 2016 to December 2019) and studied the time series of the backscatter coefficients to identify deforested areas in the Brazilian Amazon. They obtained 94% of accuracy with MLC and 96% with AT. However, a comprehensive performance analysis comparing training and validation data was not addressed in that procedure. In our approach, the aim is to assess the classification capability of the NN algorithm to detect deforested areas based on different spatial statistical characteristics of the backscatter coefficient trend. In addition, machine learning algorithms have been proved more appropriate than traditional statistical algorithms for the classification of

remote sensing data (Benediktsson et al., 1990). This work, therefore, presents a method to discriminate deforested areas over the Brazilian Amazon based on NN and Sentinel-1 SAR images. To our best knowledge, the scientific community has not explored this approach to detect near real-time deforestation over the Brazilian Amazon. This paper is organized as follows: Section 2 provides details of the data set and the chosen NN. Section 3 presents the main results obtained, while the results are discussed in Section 4. The concluding remarks are presented in Section 5.

Material and methods

Study area

The study area encompasses part of the municipalities of Altamira, Itaituba, and Novo Progresso, southwest of Pará State, a region with the highest deforestation rates in this state (Figure 3). This region is considered a hotspot in terms of human occupation and is one of the main frontiers of deforestation in the deforestation arch.

Sentinel-1 data set

For this research, we selected Sentinel-1A, Single Look Complex (SLC) images acquired in the Interferometric Wide (IW) swath mode from the European Copernicus program with a free and open data distribution policy (Open Access Hub, n.d.; Potin et al., 2019). The Sentinel-1A operates at a C-band (5.3 cm wavelength) and a swath width of 250 km (Torres et al., 2012). We selected one image every 12 days, dual-polarization (VV and VH), descendent mode, from the years 2019 to 2018, i.e. a total of 30 images per year (Table 1). The incidence angle ranged from about 29° to 46° and the resolution was about 5 m in range and 20 m in azimuth (ESA, 2021).

The SAR images were pre-processed by means of Sentinel Application Platform (SNAP), an open-source software developed by the European Space Agency (ESA; SNAP Download, n.d.). The pre-processing operations included orbit file correction, thermal noise removal, radiometric calibration (Sigma0), de-burst, and speckle filtering by the Gamma-Map filter. For terrain correction, we used external data of 30-m spatial resolution, obtained from AW3D digital elevation model (DEM) ("ALOS Global Digital Surface Model 'ALOS World 3D – 30 m' (AW3D30)" n.d.). As a result, we obtained images with an approximate spatial resolution of 14.05 m (WGS84, UTM) converted into backscattering coefficients (σ°, units in dB).

Forested and deforested sampling

Table 2 shows the selected Sentinel-2 overpasses from May to October of 2019 that were used to visually select areas without deforestation (FF) and areas with

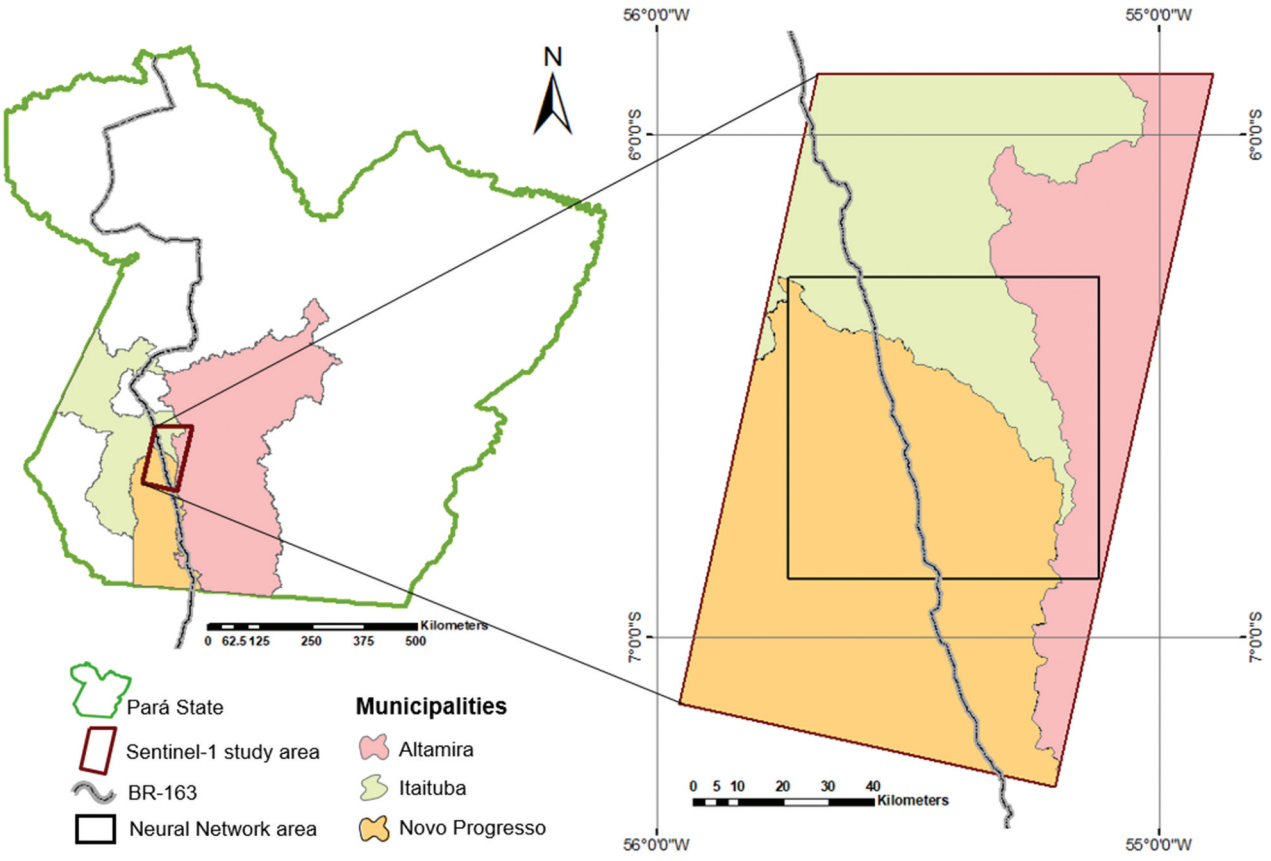

Figure 3. Location of the study area in the Pará State, along the BR-163 highway.

Table 1. Sentinel-1A interferometric wide (IW), single look complex (Level 1) overpasses from 2019 to 2018 considered in this study.

Overspass 2019	Scene Identification 2019	Overspass 2018	Scene Identification 2018
Jan-03	S1A_IW_SLC_1SDV_20190103T092340	Jan-08	S1A_IW_SLC_1SDV_20180108T092333
Jan-15	S1A_IW_SLC_1SDV_20190115T092340	Jan-20	S1A_IW_SLC_1SDV_20180120T092333
Feb-08	S1A_IW_SLC_1SDV_20190208T092339	Feb-01	S1A_IW_SLC_1SDV_20180201T092333
Feb-20	S1A_IW_SLC_1SDV_20190220T092339	Feb-13	S1A_IW_SLC_1SDV_20180213T092332
Mar-04	S1A_IW_SLC_1SDV_20190304T092339	Feb-25	S1A_IW_SLC_1SDV_20180225T092332
Mar −16	S1A_IW_SLC_1SDV_20190316T092339	Mar-09	S1A_IW_SLC_1SDV_20180309T092332
Mar −28	S1A_IW_SLC_1SDV_20190328T092339	Mar-21	S1A_IW_SLC_1SDV_20180321T092332
Apr-09	S1A_IW_SLC_1SDV_20190409T092339	Apr-02	S1A_IW_SLC_1SDV_20180402T092333
Apr-21	S1A_IW_SLC_1SDV_20190421T092340	Apr-14	S1A_IW_SLC_1SDV_20180414T092333
May-03	S1A_IW_SLC_1SDV_20190503T092340	Apr-26	S1A_IW_SLC_1SDV_20180426T092334
May-15	S1A_IW_SLC_1SDV_20190515T092341	May-08	S1A_IW_SLC_1SDV_20180508T092334
May-27	S1A_IW_SLC_1SDV_20190527T092341	May-20	S1A_IW_SLC_1SDV_20180520T092335
Jun-08	S1A_IW_SLC_1SDV_20190608T092342	Jun-01	S1A_IW_SLC_1SDV_20180601T092336
Jun-20	S1A_IW_SLC_1SDV_20190620T092343	Jun-13	S1A_IW_SLC_1SDV_20180613T092337
Jul-02	S1A_IW_SLC_1SDV_20190702T092344	Jun-25	S1A_IW_SLC_1SDV_20180625T092337
Jul-14	S1A_IW_SLC_1SDV_20190714T092344	Jul-07	S1A_IW_SLC_1SDV_20180707T092338
Jul-26	S1A_IW_SLC_1SDV_20190726T092345	Jul-19	S1A_IW_SLC_1SDV_20180719T092339
Aug-07	S1A_IW_SLC_1SDV_20190807T092346	Jul-31	S1A_IW_SLC_1SDV_20180731T092339
Aug-19	S1A_IW_SLC_1SDV_20190819T092347	Aug-12	S1A_IW_SLC_1SDV_20180812T092340
Aug-31	S1A_IW_SLC_1SDV_20190831T092347	Aug-24	S1A_IW_SLC_1SDV_20180824T092341
Sep-12	S1A_IW_SLC_1SDV_20190912T092348	Sep-05	S1A_IW_SLC_1SDV_20180905T092341
Sep-24	S1A_IW_SLC_1SDV_20190924T092348	Sep-17	S1A_IW_SLC_1SDV_20180917T092342
Oct-06	S1A_IW_SLC_1SDV_20191006T092349	Sep-29	S1A_IW_SLC_1SDV_20180929T092342
Oct-18	S1A_IW_SLC_1SDV_20191018T092348	Oct-11	S1A_IW_SLC_1SDV_20181011T092342
Oct-30	S1A_IW_SLC_1SDV_20191030T092349	Oct-23	S1A_IW_SLC_1SDV_20181023T092342
Nov-11	S1A_IW_SLC_1SDV_20191111T092349	Nov-04	S1A_IW_SLC_1SDV_20181104T092342
Nov-23	S1A_IW_SLC_1SDV_20191123T092348	Nov-16	S1A_IW_SLC_1SDV_20181116T092342
Dec-05	S1A_IW_SLC_1SDV_20191205T092348	Nov-28	S1A_IW_SLC_1SDV_20181128T092341
Dec-17	S1A_IW_SLC_1SDV_20191217T092347	Dec-10	S1A_IW_SLC_1SDV_20181210T092341
Dec-29	S1A_IW_SLC_1SDV_20191229T092347	Dec-22	S1A_IW_SLC_1SDV_20181222T092341

deforestation (FD). We collected samples over homogeneous areas (at least 90%) in terms of primary forest and clear-cut deforestation, located in flat topography. The presence of forest was guaranteed by evaluating Sentinel-2 images from 2018 to 2020 (25 August 2018 image and 20 June 2020). The 98 FF samples presented an average size of 95 pixels, while the 199 FD samples presented an average size of 66 pixels (Figure 4).

For each FF and FD sample, the mean, standard deviation, and maximum-minimum difference (MMD), that is the difference between the maximum and minimum value of the backscatter coefficient, were calculated for both VH and VV polarizations. The metrics were computed over the polygons for each acquisition in the year 2019. Figure 5 shows an example of each statistical parameter for FF and FD areas in the VH and VV polarizations. For every acquisition, shown on the horizontal axis, the related statistical value is reported on the y-axis. In this way, the variation of the statistical parameter throughout the year can be obtained and used to discriminate the forested area from the deforested area.

Table 2. Forest–Deforested and Forest–Forest samples (FD) manually collected based on Sentinel-2 images acquired in 2019.

Time interval	Number of samples FD	Number of samples FF
May 7–June 16	58	
Jun 16–Jun 21	1	
Jun 21–Jun 26	8	
Jun 26–Jul 16	35	
Jul 16–Jul 21	15	
Jul 21–Jul 31	21	
Jul 31–Aug l0	16	
Aug 10–Aug 20	10	
Aug 20–Aug 30	14	
Aug 30–Sep 9	8	
Sep 9–Sep 19	13	
Sep 19–Oct 9	1	
Total	199	99

Multi-layer perceptron (MLP)

An artificial NN may be viewed as an adaptive model of nonlinear parallel processing units massively interconnected. The NNs are capable of acquiring knowledge from the surrounding environment through a process of learning which modifies the interconnection weights between the units. Therefore, NNs can learn from the training examples by constructing input-output mappings. This learning ability allows NNs to generalize, i.e. to produce good approximations of outputs from inputs not found during the learning phase (Haykin, 2009). The processing unit is the elementary block of the NNs, which is mainly characterized by its activation function. The latter is essential in NNs because it adds the nonlinearity that makes them capable of learning complex patterns (Sharma et al., 2020).

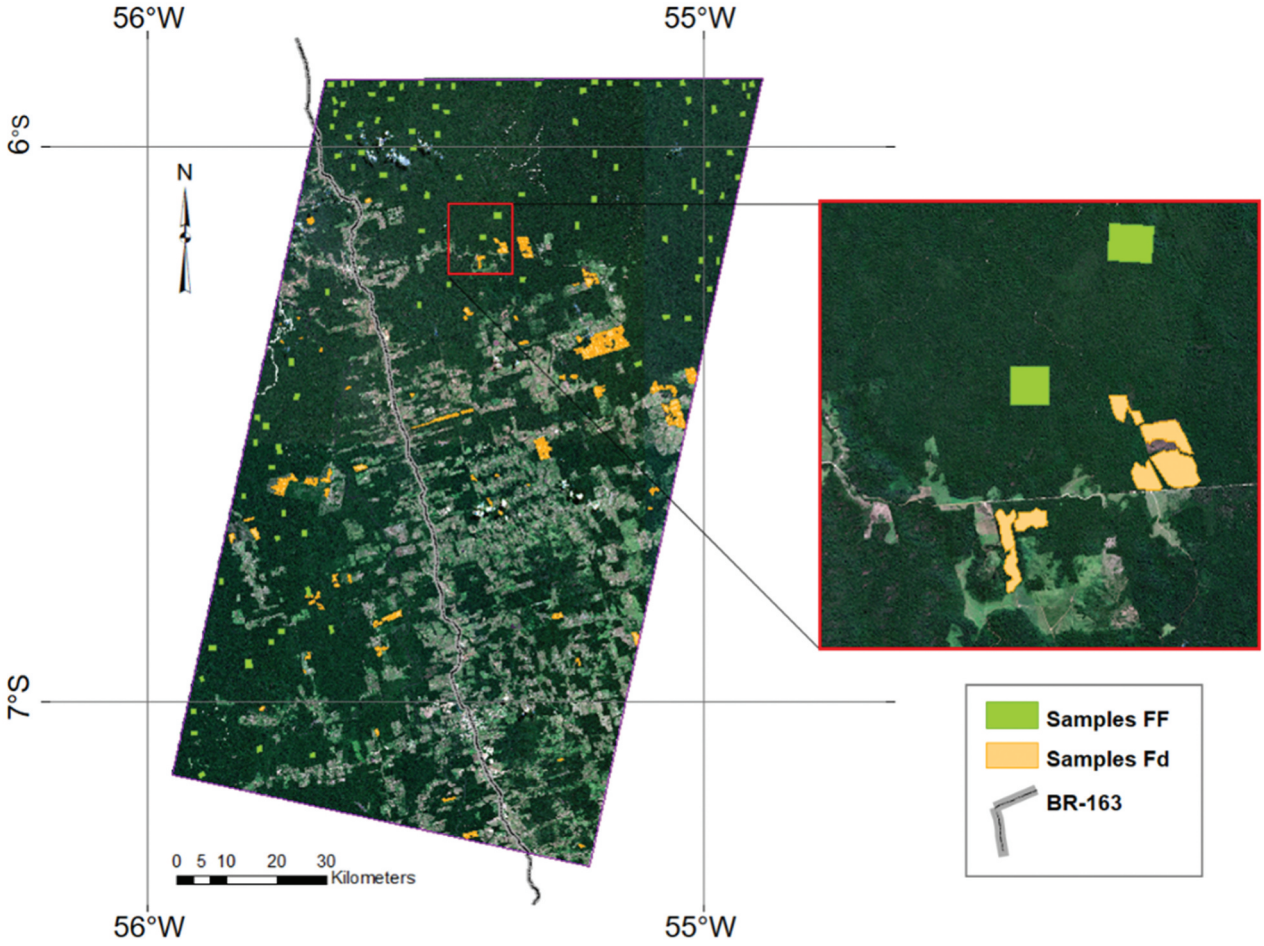

Figure 4. Example of Forested–Forested (FF) and Forested–Deforested (FD) samples manually collected in different overpasses of Sentinel-2 satellite, overlaid on the RGB color composite of bands 4, 3, and 2 of Sentinel-2 satellite image obtained in 1 July 2019.

NNs can be distinguished by their architectures or structures. In this study, we considered the MLP. MLP is a feedforward NN, i.e. the input is projected unidirectionally to the output, which is distinguished by the presence of one or more hidden layers between the input and output layers. MLPs are applied in classification and regression problems in many fields, including remote sensing (Ramchoun et al., 2016). Since we implemented a binary classifier, a sigmoid activation function was used for the final layer. It outputs a value between 0 and 1 that can be treated as a probability that the given input belongs to a particular class (Sharma et al., 2020).

The number of hidden layers and units depends on the specific problem and cannot be determined a priori (Ramchoun et al., 2016). In this study, we applied two hidden layers of units between the input vector with the measured features and the output vector with the classification response (Del Frate & Solimini, 2004). The initial number of units was estimated following the study conducted by Del Frate and collaborators and was defined for each specific case. The MLP topology consists of four layers (Figure 6). As discussed in detail in Section 2.5, four case studies with different input configurations were analysed. Therefore, we designed four MLP topologies with the number of input and hidden units varying depending on the case study.

Data set preparation

The statistical features extracted from the FD and FF sample areas were inputs to the NN, trained to automatically detect the probability that an area was deforested. Different case studies were considered to form the input vectors. First, the statistical parameters were involved individually, and then a combination of them was considered. Specifically, four different sets of inputs were chosen:

(1) mean σ° values of both VV and VH polarizations;
(2) mean σ° values and corresponding standard deviation of both VV and VH polarizations;
(3) mean σ° values and corresponding MMD values of both VV and VH polarizations; and
(4) mean σ° values and corresponding standard deviation and MMD of both VV and VH polarizations.

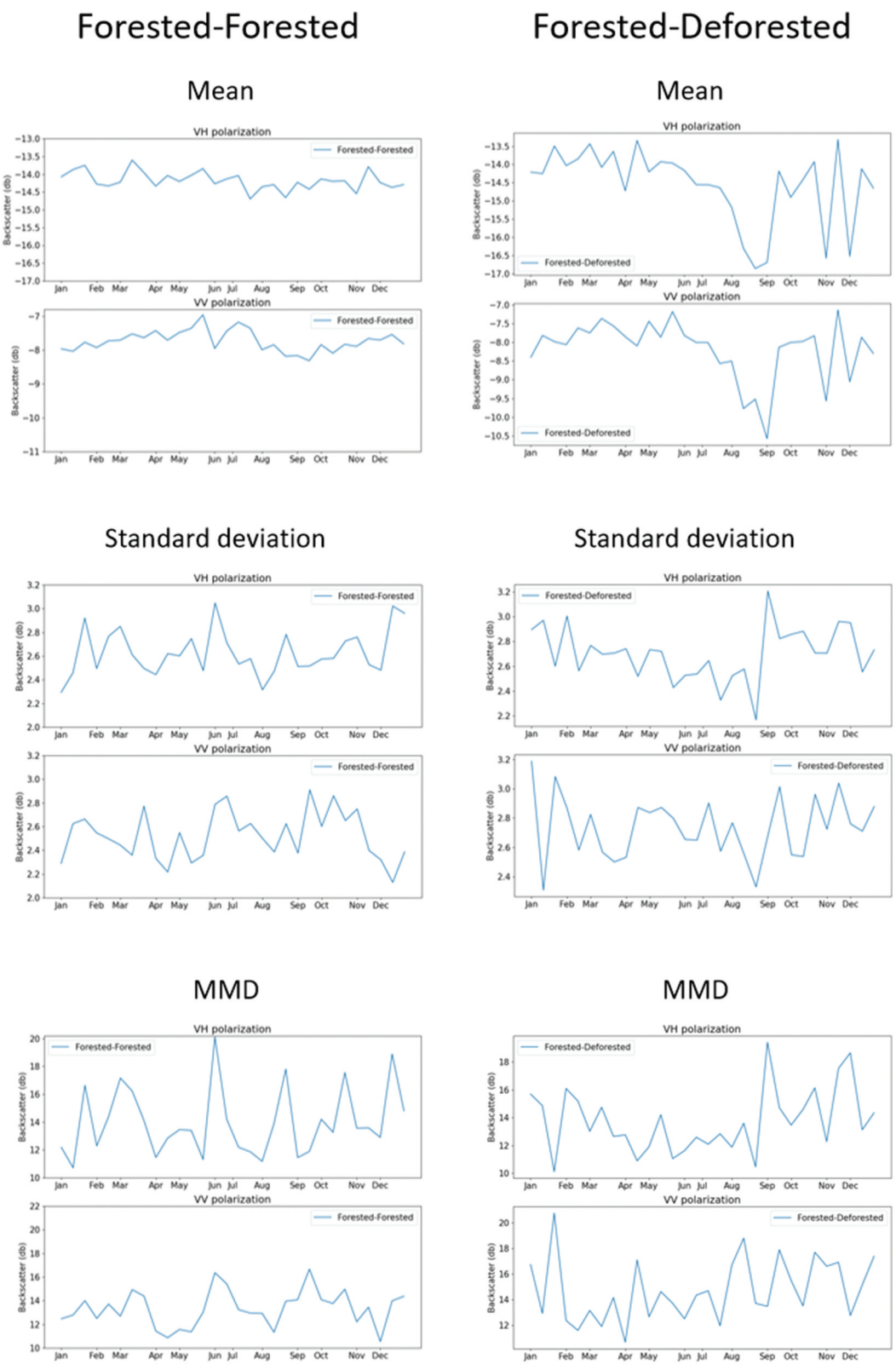

Figure 5. Mean, standard deviation, and MMD (maximum-minimum difference) example of the backscatter coefficient in VH and VV polarizations.

Standard deviation and MMD were not considered individually as they did not exhibit good performances. Similarly, preliminary results obtained with single polarization configurations suggested disregarding such an option. Figure 7 shows the processing procedure, which is the same for the four case studies.

As a first step in the data set construction, the number of samples related to the FF condition was equalized to the FD ones by increasing the former through a data augmentation process. More specifically, synthetic data (noisy data) was generated from the original data (seeds) by adding slightly modified copies of them.

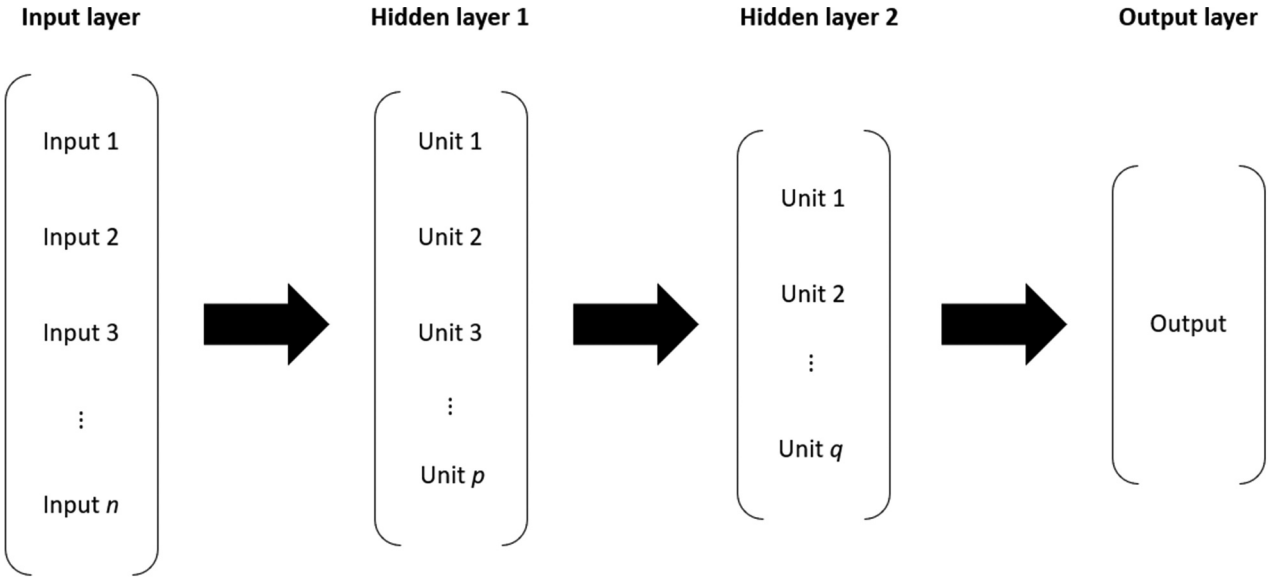

Figure 6. Multi-Layer Perceptron topology, n, p, and q represent the total number of units in the input and hidden layers that change accordingly in the considered case study.

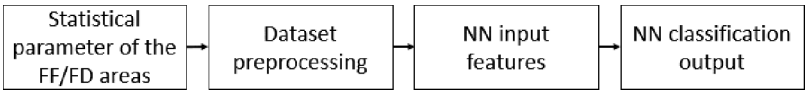

Figure 7. Block diagram showing the processing procedure.

Random noise vectors of the same size as the seeds vectors were created according to a Gaussian distribution with specific mean and variance. These two parameters were chosen due to the required similarity between the noisy vector and the original one. For the first case study, where only the mean σ° values are considered, an example of a noise vector is shown in Figure 8(a). It consists of 30 elements, as the number of features in case study (1) in the VH polarization only. The noise values range approximately from −0.3 to 0.3. The sum of the noise vector and the original seed vector is shown in Figure 8(b) for the average value of the backscatter. The original vector is shown in orange, while the noisy one in blue.

To have a data set of sufficient size to train the NN, the whole number of input samples (both FD and FF samples) was increased in a similar way. The data set generation results for the case study (1) (average value of the backscatter coefficient) are shown in Table 3. In this case, the data set was enlarged five-fold to obtain

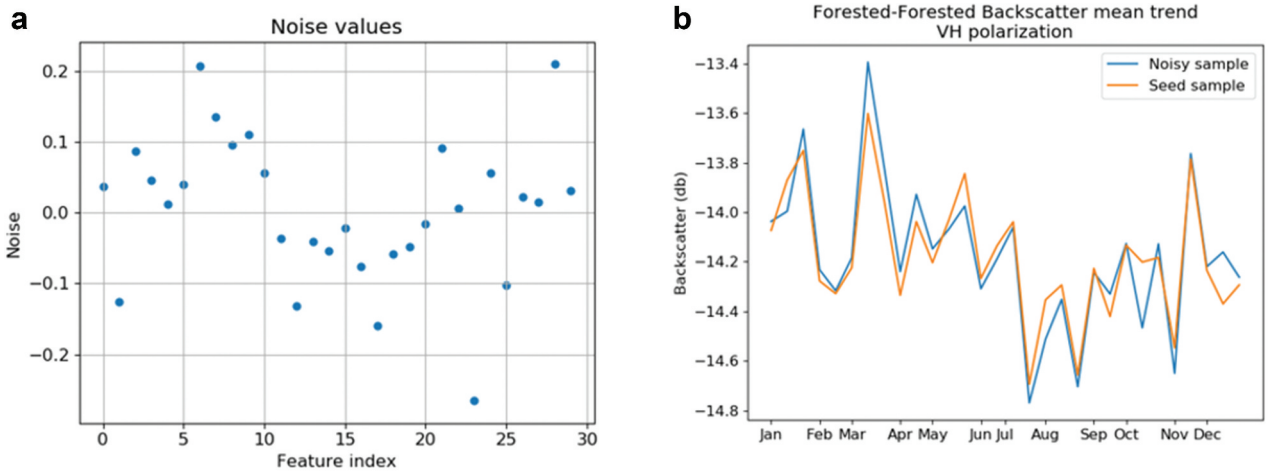

Figure 8. Random noise values generated (a) and the "seed" (shown in Orange) and noisy (shown in blue) samples for VH polarization (b).

Table 3. Training data set description after augmentation (case study 1: mean σ° values).

Parameters	Forested–Deforested (FD)	Forested–Forested (FF)
Number of acquisitions per year	30	30
Polarizations	VH and VV	VH and VV
Number of areas (for each acquisition)	199	98 x 3 = 294 (199 selected)
Augmented number of areas	199 x 5 = 995	199 x 5 = 995
Number of samples	199 + 995 = 1194	199 + 995 = 1194

Table 4. Description and number of the case study features. MMD = maximum-minimum difference.

Case study	Features	Total number of features
1	30 mean VH + 30 mean VV	60
2	30 mean VH + 30 SD VH + 30 mean VV + 30 standard deviation VV	120
3	30 mean VH + 30 MMD VH + 30 mean VV + 30 MMD VV	120
4	30 mean VH + 30 standard deviation VH + 30 MMD VH + 30 mean VV + 30 standard deviation VV + 30 MMD VV	180

a total number of samples equal to 1194 + 1194 = 2388. Since the statistical features differ significantly, each sample was normalized between 0 and 1 before being input to the NN.

Each sample in the data set is described by features related to the backscatter coefficient in the VH and VV polarizations. The number of features for each sample depends on the case study: for the case study (1), the features are 60 (30 VH + 30 VV features); for the case studies (2) and (3), they are 120 (60 VH + 60 VV features); and for the case study (4), they are 180 (90 VH + 90 VV features). Table 4 provides a summary of this split. Thus, the input of the NN is a vector with the number of entries that is equal to the number of features. Since the features differ significantly, each sample was normalized between 0 and 1.

Training phase (2019 data set)

Generally, in machine learning models, the data set is divided into three distinct parts: training, validation, and test data sets split into the proportion of 75%, 15%, and 10%, respectively. These proportions are a typical choice in machine learning data separation (Haykin, 2009). The training and validation sets are used during the training process, while the test set is used to evaluate the performance achieved. Indeed, the test set is used separately from the previous ones and is not involved in the learning procedure. In this paper, these proportions were considered for all case studies. The sample division for the first case study is reported in Table 5.

During the supervised learning process, the connection weights are optimized to minimize the error, namely the difference between the desired response and the actual response, according to a loss function. This error is evaluated both on the training and validation sets, which consists of examples not belonging to the training one. To avoid overfitting problems, i.e. to make the NN able to generalize over new patterns, the training of the network is stopped when the error on the validation data set reaches its minimum, according to the early stopping algorithm (Prechelt, 1998).

Table 5. Train, validation, and test set distribution for the case study (1).

Sampling sets	Forested–Deforested	Forested–Forested	Total
Train set	895	895	1790
Validation set	179	179	358
Test set	120	120	240
Total	1194	1194	2388

The number of units in the hidden layer was optimized for each input configuration, in terms of classification accuracy and generalization capability. Several attempts were made to select the proper number of units in the hidden layers which finally led to the topologies summarized in Table 6.

Evaluation of the 2018 data set

The NN capability achieved during the training phase is applied to novel input data. The trained model is used for the automatic recognition of areas deforested during the year 2018. The properties of the data set used in this phase are similar to those of the training data set: it was composed of 30 pre-processed Sentinel-1 images acquired over the same area with the same spatial resolution, which shows the σ° values for the VH and VV polarizations.

Each image of the time series was automatically divided into sub-images with a size of 10 × 10 pixels, resulting in 223,725 patches for each acquisition. Considering the pixel resolution of the S1 images of 14.05 m, 10 pixels × 10 pixels makes an area of approximately 2 ha. Table 7 shows an overview of the data set dimension. The statistical parameters were calculated for each patch for both polarizations, as described in Section 2.5, and the same four case studies were considered. Therefore, the input of the trained NN is a vector with a number of entries depending on the examined case study.

Table 6. MLP topology for each case study.

Case study	Number of units in the input layer	Number of units in the first hidden layer	Number of units in the second hidden layer	Number of units in the output layer
1	60	20	5	1
2	120	30	5	1
3	120	30	5	1
4	180	40	10	1

Table 7. Data set description of selected Sentinel-1 images from 2018.

Parameter	Specification
Number of acquisitions per year	30
Number of patches (for each acquisition)	223,725
Polarizations	VH and VV

Results evaluation

The sigmoid activation function in the NN output layer returns a class probability in the interval $[0, 1]$. A predicted value equal to or close to 0 means that the model identifies an area as forested (FF); conversely, a prediction equal to or close to 1 indicates a deforested area (FD). To evaluate the results, the confusion matrix was computed, and accuracy, precision, recall, and F1 score were derived. They are defined as (Equations 1–4):

$$Accuracy = \frac{TP + TN}{TP + FP + TN + FN} \quad (1)$$

$$Precision = \frac{TP}{TP + FP} \quad (2)$$

$$Recall = \frac{TP}{TP + FN} \quad (3)$$

$$F1 = 2 \times \frac{Precision \times Recall}{Precsion + Recall} \quad (4)$$

Where:

TP = True positives, i.e. the number of deforested areas classified as deforested.

TN = True negatives, i.e. the number of forested areas classified as forested.

FP = False positives, i.e. the number of forested areas classified as deforested.

FN = False negatives, i.e. the number of deforested areas classified as forested.

Results

Figure 9 shows an example of the multitemporal backscattering coefficients from an area that faced clear-cut deforestation between 7 May 2019 (a) and 16 June 2019 (c) for both VH (b) and VV (d) polarizations. The backscatter signal of deforestation presents a short increase followed by a sharply decreased in both polarizations until approximately 3 months (roughly, 31 August 2019). Then, the signals tended to increase after September.

From all FD samples collected in 2019, an average decrease of the mean backscatter coefficients of approximately 2 dB for VV polarization and 2.3 dB for VH polarization can be observed after deforestation. This decrease in the backscatter signal remains evident for the next 3–4 months approximately. After this period, we observed an irregular increase in both polarizations.

2019 data set

Table 8 reports the results achieved for the four case studies for the data sets obtained in 2019. The mean, standard deviation, and MMD input set showed accuracy and F1 score of 99%. The other case studies also achieved promising results: the accuracy obtained using mean and MMD slightly decreased to 98%. Lastly, mean and standard deviation, as well as mean, only showed an accuracy of 97%. False positives and false negatives were also very low. They were evaluated through the F1 metric, which is the harmonic mean of precision and recall. This means that the algorithm avoids, to a great extent, false alarms and, in most cases, does not miss the deforested areas.

2018 data set

To assess the NN performance, the 2018 results were validated using two ground truth images provided by the MapBiomas and PRODES projects. MapBiomas produces annual LULC maps by applying Random Forest classification overall Landsat scenes acquired in a specific year. The LULC maps are pixel-based, with a minimum mapping area of 1 ha. PRODES provides the annual rates of clear-cut deforestation with a minimum mapping area of 6.25 ha. PRODES makes use of moderate spatial resolution from Landsat-8, CBERS-4, and Sentinel-2 with 30 m, 20 m, and 10 m of spatial resolutions, respectively.

The data from MapBiomas and PRODES considered only deforested areas from 2018 found in the same region of the Sentinel-1 data set. The ground truth images were clipped into patches with the size of 10 pixels × 10 pixels, following the image division used for the SAR data set obtained in 2018. Each patch in the ground truth image is geographically related to the patch in the Sentinel-1 imagery in the data set. Out of the total, the ground truth patches reporting areas deforested in 2018 represent approximately 0.3% in MapBiomas while in PRODES they represent 0.6%.

The predictions related to 2018 deforested patches were collected, and the same number of predictions related to forested patches is selected randomly from the total to create a well-balanced data set. Table 9 shows the results achieved for the 2018 images for the four case studies.

Compared with the results obtained in 2019, all evaluation parameters decreased for the data sets obtained in 2018, especially for the recall, due to the relatively high number of false negatives. The recall decreased for the PRODES data. For both reference

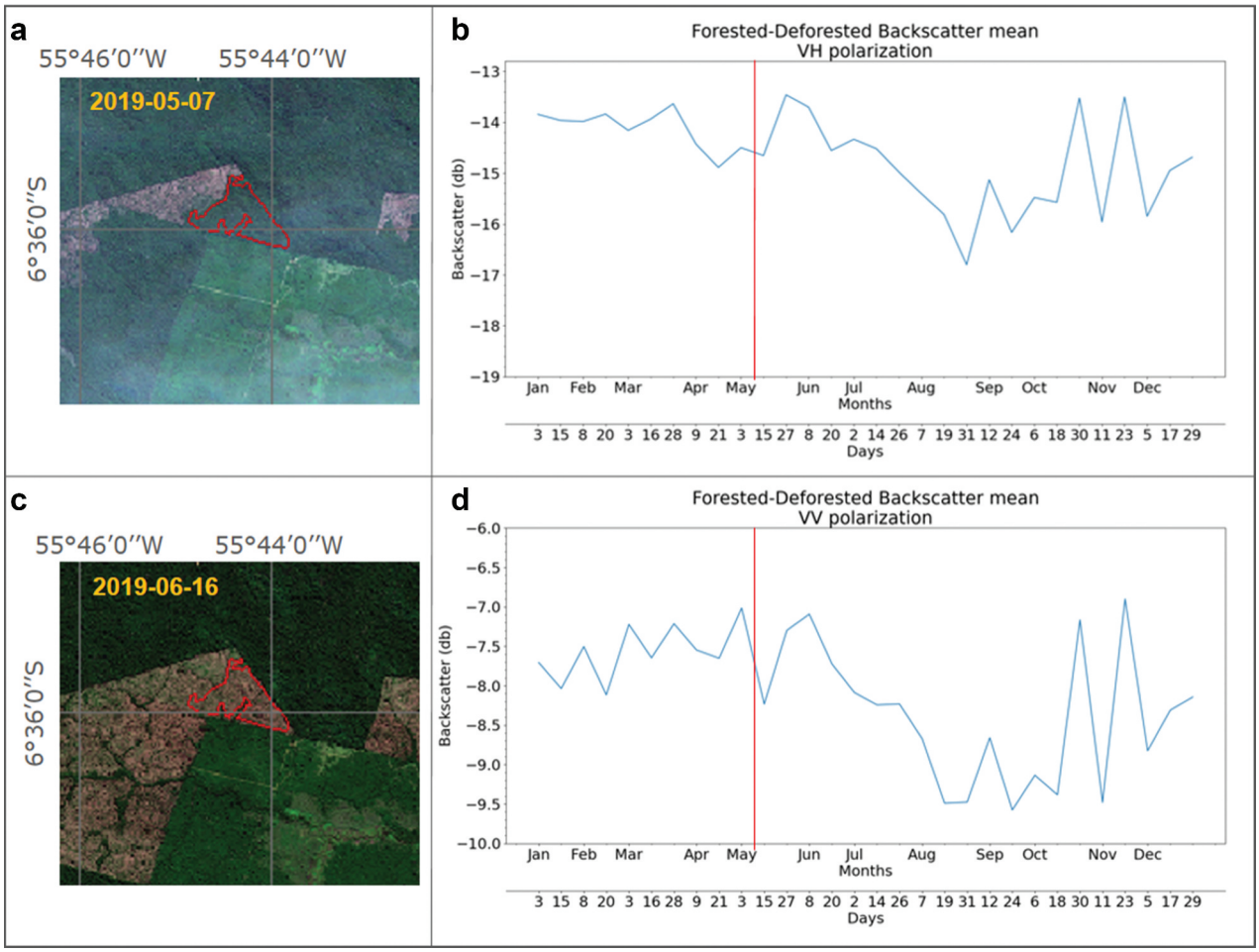

Figure 9. Left: Example of a deforested area in the study area shown by the Sentinel-2, RGB color composites of bands 4, 3, and 2 acquired on 7 May 2019, and 16 June 2019. Right: Sentinel-1 mean backscatter coefficients along the year 2019 in the VH and VV polarizations. The red line highlights the backscatter position coincident with the first data of the optical image before deforestation.

Table 8. Statistical results for the data sets obtained in 2019. MMD = maximum-minimum difference.

Statistical parameters	Accuracy	Precision	Recall	F1
Mean	0.97	0.98	0.97	0.97
Mean + standard deviation	0.97	0.99	0.94	0.97
Mean + MMD	0.98	0.96	0.99	0.98
Mean + standard deviation + MMD	0.99	0.99	0.98	0.99

data, the best-case scenario corresponded to the case study that considered mean, standard deviation, and MMD as input. In this case, the model achieved accuracy and F1 score of 89%, with a low number of false positives and false negatives, validating with the MapBiomas ground truth image and accuracy and F1 score of 81% and 79%, respectively, with the PRODES ground truth. The second best case was obtained for the mean backscatter coefficient as input parameter. The model performance declined when mean and standard deviation and mean and MMD were considered.

Discussion

In this study, we proposed a method based on NNs that detects deforested areas by analysing the annual trend of specific statistical parameters related to the backscatter coefficients obtained from Sentinel-1 images. Different statistical parameters, i.e. different case studies including mean, standard deviation, and MMD of the backscatter coefficient in VH and VV polarizations were considered. This method analysed 2 years of data sets: 2019 and 2018. Areas deforested in 2019 were manually selected, labelled, and used to train and test the algorithm, while the trained NN automatically identified areas deforested in 2018.

Figures 10, 11, 12, and 13 represent samples extracted from the 2019 data set. Figures 10 and 11 report two FF areas, while Figures 12 and 13 report FD areas. On the left, the figures illustrate the RGB colour composites (a, c) obtained from Sentinel-2 2019 images. The right shows the related mean backscatter trend in both VH (b) and VV (d) polarizations.

Table 9. Statistical results for the ground truth data sets obtained in 2018. SD = standard deviation. MMD = maximum-minimum difference.

	MapBiomas				PRODES			
Parameter	Accuracy	Precision	Recall	F1	Accuracy	Precision	Recall	F1
Mean	0.85	0.88	0.81	0.85	0.79	0.87	0.67	0.76
Mean + SD	0.88	0.96	0.79	0.87	0.78	0.95	0.58	0.72
Mean + MMD	0.85	0.87	0.82	0.85	0.76	0.84	0.64	0.73
Mean + SD + MMD	0.89	0.90	0.89	0.89	0.81	0.88	0.73	0.79

The VV and VH signals from the Forested–Forested samples (depicted in Figures 10 and 11) show regularity of the signal for both polarizations with the mean backscatter signal values from −14.2 dB for VH and −7.7 dB for VV polarizations. When deforestation occurs, the VV and VH backscatter signals are perturbed. After deforestation, it was observed a short increase of the backscatter signal before a more pronounced decrease. From all samples collected, we observed an average decrease of 2.3 dB for VH and 2 dB for VV polarizations. The decrease was evident and lasted from about 3 to 4 months. Some authors have observed the increase and decrease of the backscatter signal after deforestation (Bouvet et al., 2018; Doblas et al., 2020; Hoekman et al., 2020; Joshi et al., 2015; Kellndorfer, 2019; Reiche et al., 2018a, 2018b).

Reiche et al. (2018a) found a decrease of 2.0 dB in VH after deforestation in the province of Riau, Indonesia, through Sentinel-1 C-band SAR data time-series. Reiche et al. (2018b) observed a decrease of 2.5 dB, using VV time-series of Sentinel-1, from deforestation studies in the province of Santa Cruz, Bolivia.

Bouvet et al. (2018) stated that the C-band SAR backscatter signal over cleared or burned areas presents a lower backscatter signal of ~2.5 dB in the Amazon rainforest in Peru. Decrease backscattering was also observed for the majority of our deforested areas collected in 2019.

Hoekman et al. (2020) reported that, in general, undisturbed forests have a relatively high and stable backscatter level; therefore, a significant decrease in backscatter level would indicate deforestation. The backscatter of clear-cut areas, in both polarizations, is

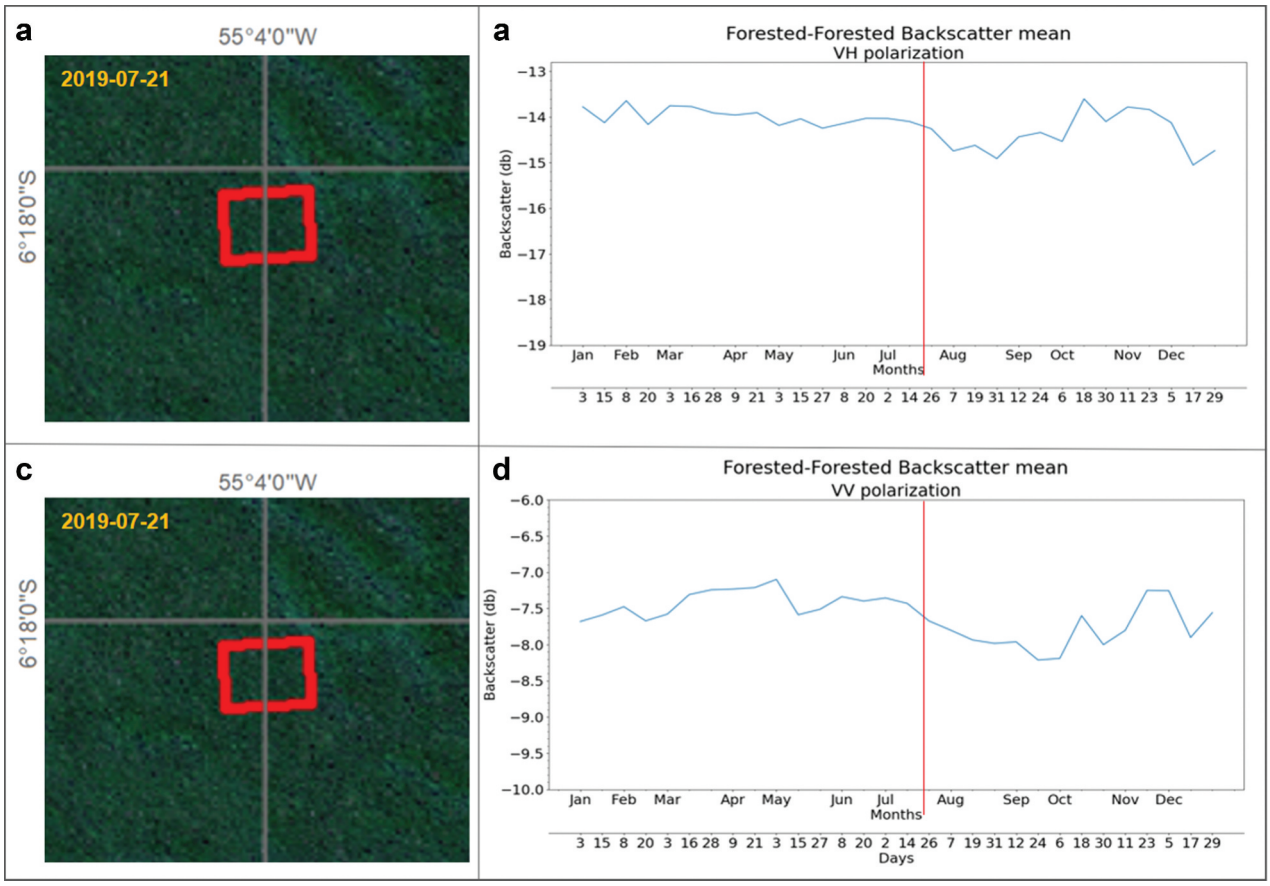

Figure 10. Sentinel-2 RGB colour composite (a, c) acquired on 21 July 2019 of a Forested–Forested sample (highlighted in red), and backscatter mean trend in VH (b) and VV (d) polarizations. The red line highlights the backscatter position coincident with the data of the optical image.

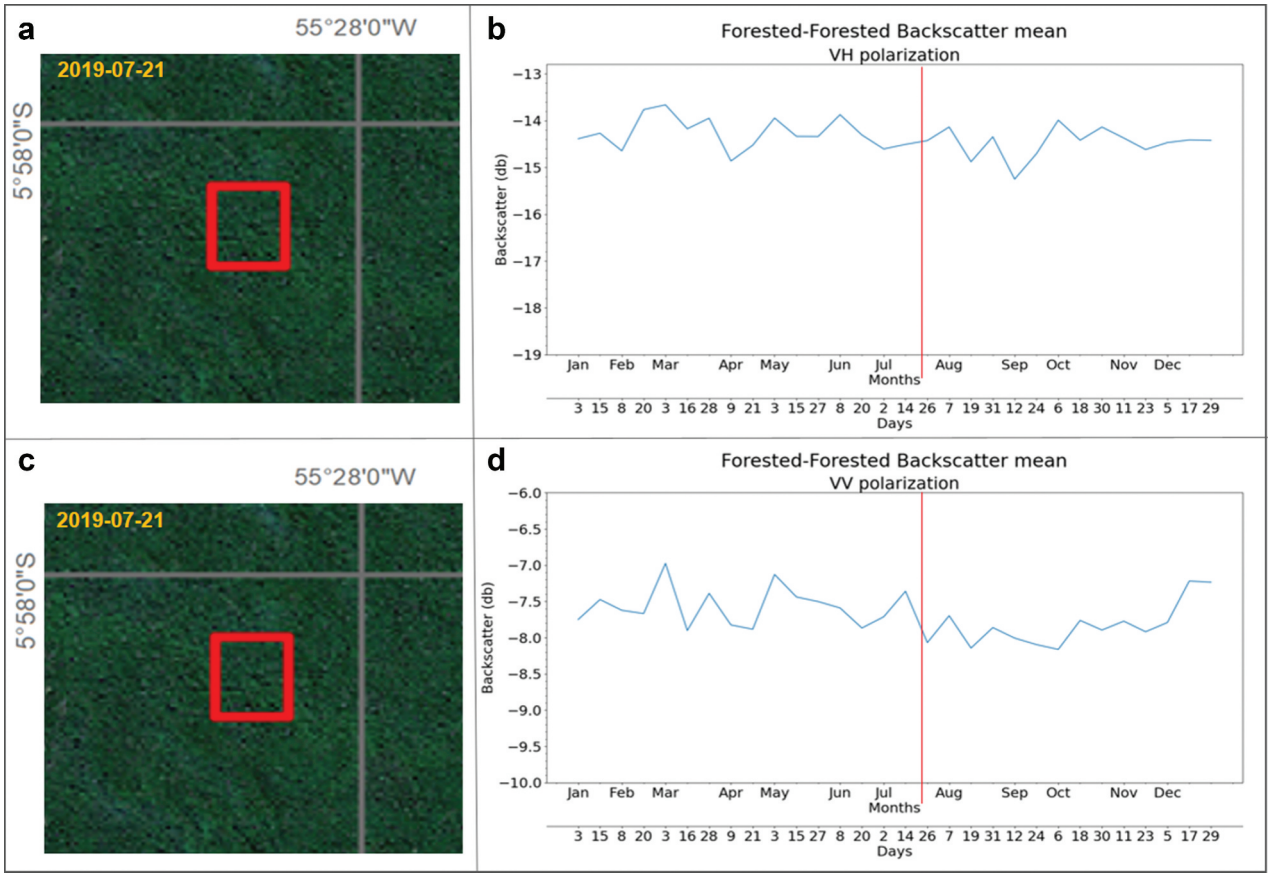

Figure 11. Sentinel-2 RGB colour composite (a, c) acquired on 21 July 2019 of a Forested–Forested sample (highlighted in red), and backscatter mean trend in VH (b) and VV (d) polarizations. The red line highlights the backscatter position coincident with the data of the optical image.

usually 2.0 dB lower than the original forest cover. However, remaining debris and undergrowth, terrain slopes, soil roughness, and soil moisture may intensify the decrease. The rainforest site in the Indonesian province of Central Kalimantan and in the Pará State, Brazil, Hoekman et al. (2020) observed that VH and VV signals go up and down, and deforestation was characterized at the first moment the signal goes down.

Joshi et al. (2015) revealed an L-band backscatter decrease of 1.1 dB in VH after clearing full forest cover events in the region of Madre de Dios in Peru.

Doblas et al. (2020), in a study in the Amazon rainforest, determined the mean backscattering values of the forest as −12.4 and −6.25 dB for VH and VV polarizations, respectively, while the mean backscattering values of the deforested series are consistently lower, reaching −13.1 and −7.6 dB for VH and VV polarizations.

For the 2019 test data set, the NN model achieved high performance in all case studies. This was due to the manual selection and labelling of the test areas employing the RGB composition of Sentinel-2 images. For the 2018 data set, the performance decreased, as shown in Figure 14 that reports the trend of the F1 metric for the four case studies from 2019 to 2018 images.

To investigate the 2018 results, three deforested areas among the largest ones in the ground truth images were analysed. Figures 15, 16, and 17 show the three areas. Each RGB color composition shows the areas captured by the Sentinel-2 satellite from April to July of 2018. These figures highlight the differences in land cover changes due to the clear-cutting process. At the bottom, the figures represent the ground truth images and the classification made by the MLP for the MapBiomas (b), (c), and PRODES (d), (e) ground truths. In the ground truth images (b) and (d), the areas deforested in 2018 are shown in white, areas forested are shown in black, and areas deforested before 2018 are in grey. The classification images (c) and (e) show the patches as they were classified overlapped to the ground truth image.

The F1 score differences between the PRODES and MapBiomas ground truth images may be related to the resolution employed by the two projects. The coarser PRODES resolution does not capture small deforested areas that are considered in the MapBiomas ground truth. Indeed, PRODES does not capture small forested areas inside a deforested polygon. This can explain the difference in Recall, due to the number of false negatives

between the two ground truth images. A large number of false negatives are localized in the small areas detected by the MapBiomas. Moreover, the misclassification may be caused by the deforestation method. After clear-cutting, the trees are left on the ground for drying before being burned. Since the amount of biomass remains the same, the result is somehow similar in backscatter values compared with intact forest areas. Bouvet et al. (2018), Kellndorfer (2019), and Hoekman et al. (2020) observed these trends.

Bouvet et al. (2018) reported that large branches remaining in the ground can cause a double-bounce scattering mechanism and mask the decrease of the backscatter signal. The authors also stated that, after rainfall events, the backscatter signals can exhibit the same values as intact forests.

Kellndorfer (2019) stated that if deforestation results in rough soil conditions (e.g. slash) backscatter can be significantly enhanced until logs are removed. The authors declared yet that, after deforestation, there is a dominant change from volumetric scattering to surface scattering, with an expected decrease in the cross-polarized (VH, HV) signal.

Hoekman et al. (2020) reported that deforestation in Brazil often is the slash-and-burn type of small scale, and in most instances, the deforestation is preceded by severe degradation.

Figure 18 shows examples of test sites from the Amazon forest, with slashed trees after 3 months of drying (A). As it can be seen, the site conserves all the previously standing biomass but with dried leaves and trunks. The green leaves are from liana vines that grew along with the slashed biomass (Soares Neto et al., 2009). Figure 18 also shows how a clear-cut site appears after the cleaning fire (B). Small branches and leaves are combusted to completion, while large trunks are only partially consumed (Christian et al., 2007). Long ash trails indicate trunks, mostly palm trees that were completely consumed through smouldering. However, misclassification may be associated with the deforestation method.

In this study, we implemented a new methodological flow based on Sentinel-1 data and MLP classifier capable of detecting deforestation automatically in the Amazon rainforest. The accuracy was in the range of 81% to 89%, depending on the considered

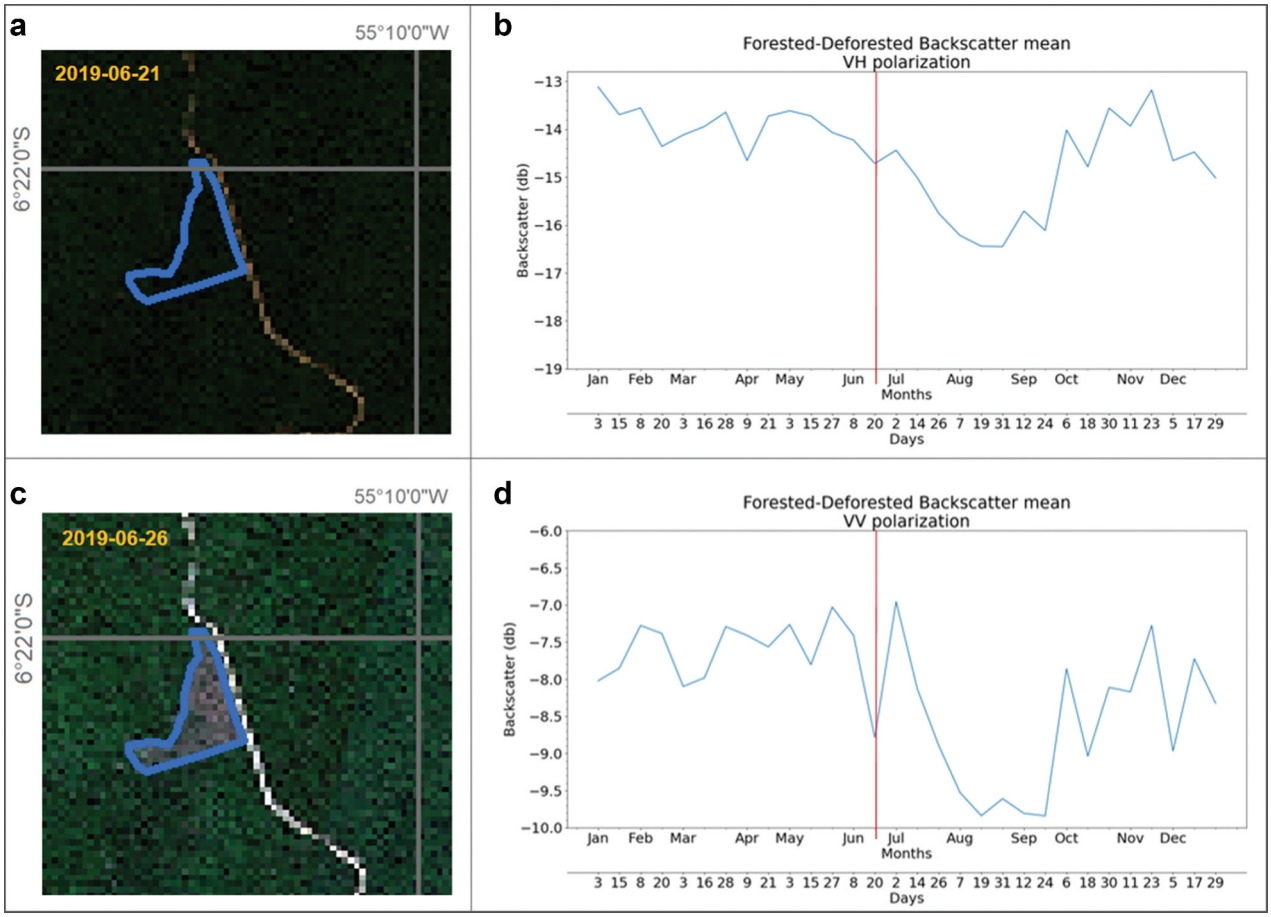

Figure 12. Sentinel-2 RGB colour composite acquired on 21 June 2019 (a) and 26 June 2019 (c) of a Forested–Deforested sample (highlighted in blue), and backscatter mean trend in VH (b) and VV (d) polarizations. The red line highlights the backscatter position coincident with the first data of the optical image before deforestation.

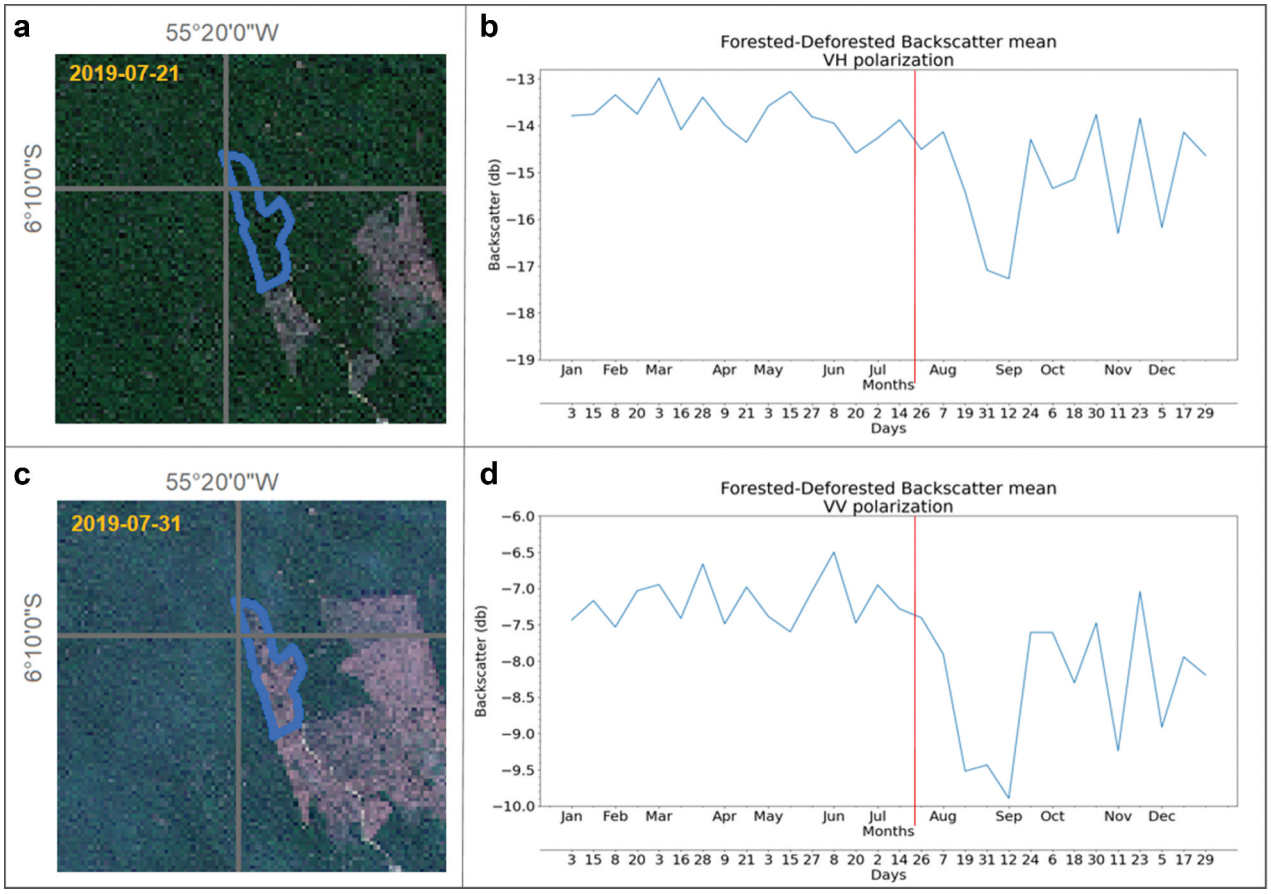

Figure 13. Sentinel-2 RGB colour composite acquired on 21 July 2019 (a) and 31 July 2019 (c) of a Forested–Deforested sample (highlighted in blue), and backscatter mean trend in VH (b) and VV (d) polarizations. The red line highlights the backscatter position coincident with the first data of the optical image before deforestation.

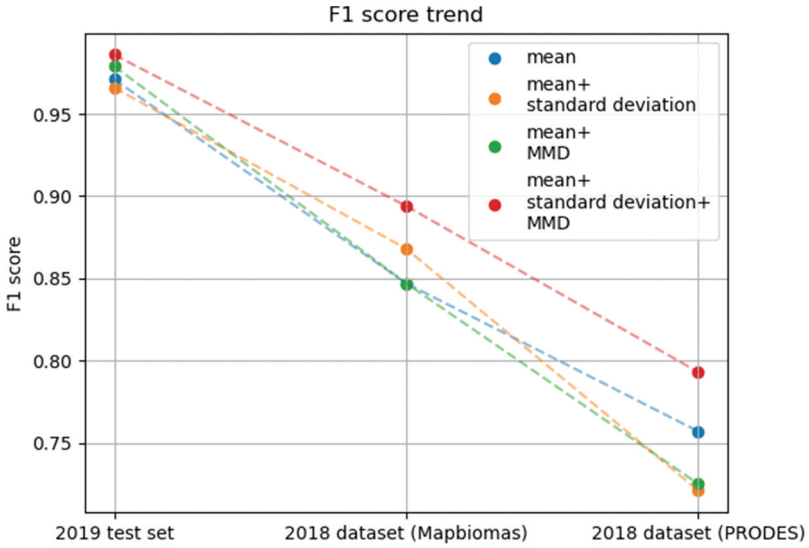

Figure 14. F1 variation for the 2019 test set and 2018 data set for both ground truth images.

reference image. In hand-picked areas used for training the NN, the accuracy reached 99%, comparable to those achieved by Bem et al. (2020), whose accuracy reached 94%. Bem et al. (2020) combined optical images and NN for detecting deforestation. The method, however, could only be applied in the dry season of the Amazon rainforest, which lasts for about 6 months. Methods based on radar data can be used throughout the year.

Doblas et al. (2020), which research is based on radar data, reached maximum accuracy of 96% in detecting deforestation. Our results are 2% higher

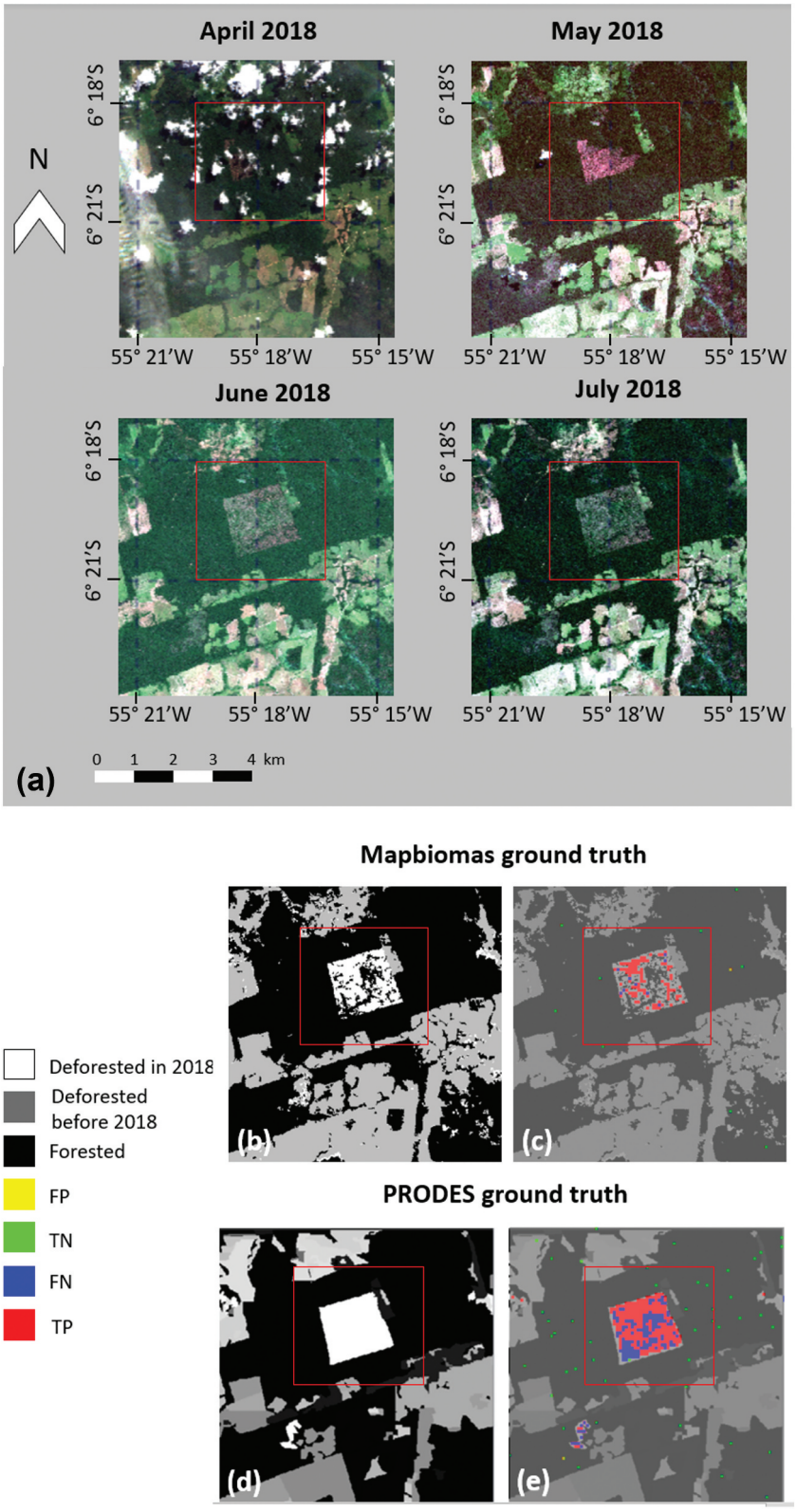

Figure 15. First example of an area with deforestation (highlighted in red), shown by the Sentinel-2 RGB color composites acquired in April, May, June, and July 2018 (a). MaBiomas ground truth (b), classification output with MapBiomas ground truth (c), PRODES ground truth (d), and classification output with PRODES ground truth (e). FP = False positives (number of forested areas classified as deforested), TN = True negatives (number of forested areas classified as forested), FN = False negatives (number of deforested areas classified as forested), and TP =True positives (number of deforested areas classified as deforested).

than the data set of 2019 and 7% lower for the 2018 images, which were obtained automatically by the algorithm.

The MLP does not require high computer processing capability compared with other NN algorithms, such as the CNNs (Bouguettaya et al., 2019). The algorithm

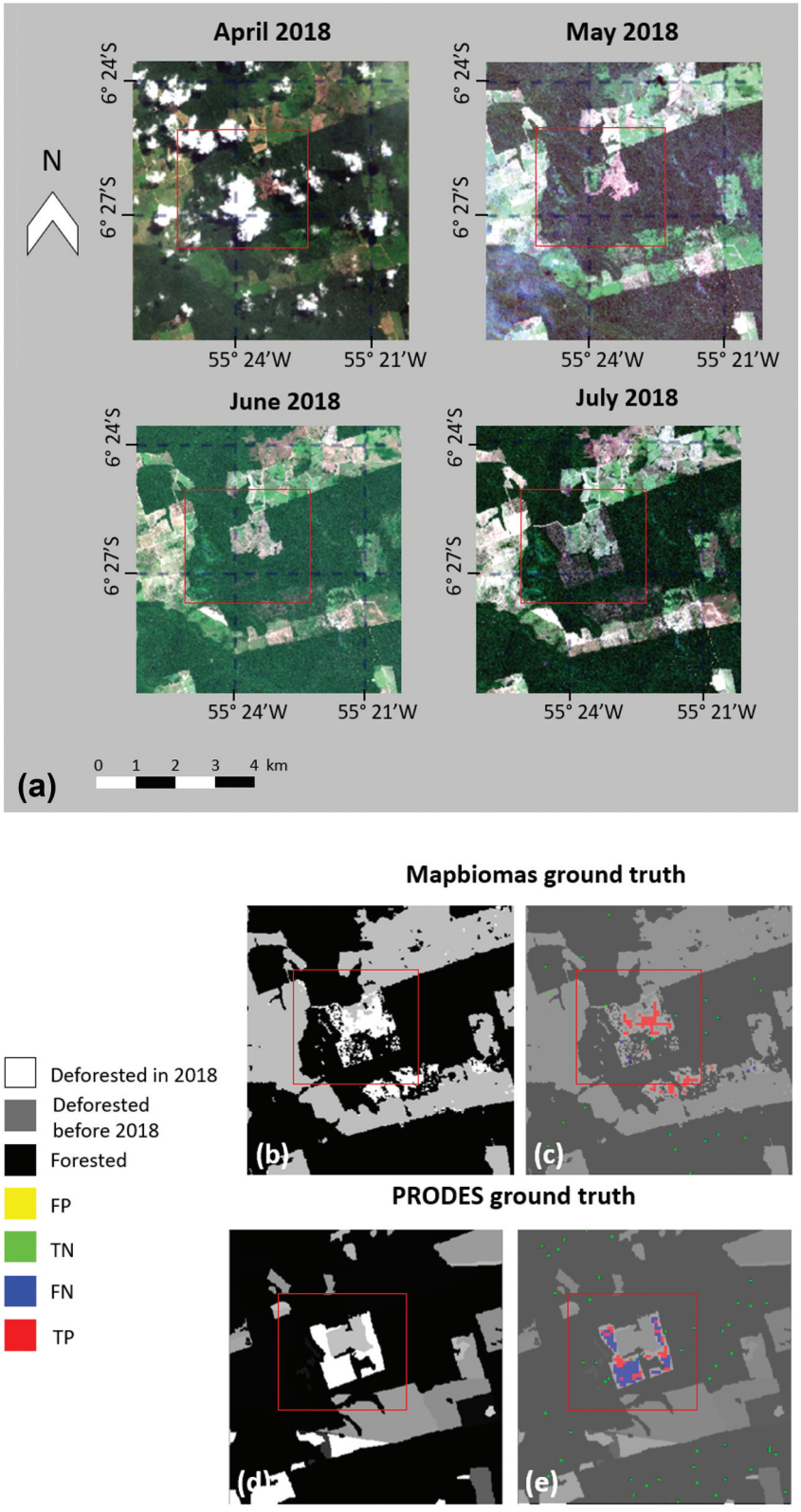

Figure 16. Second example of an area with deforestation (highlighted in red), shown by the Sentinel-2 RGB color composites acquired in April, May, June, and July 2018 (a). MapBiomas ground truth (b), classification output with MapBiomas ground truth (c), PRODES ground truth (d), and classification output with PRODES ground truth (e). FP = False positives (number of forested areas classified as deforested), TN = True negatives (number of forested areas classified as forested), FN = False negatives (number of deforested areas classified as forested), and TP =True positives (number of deforested areas classified as deforested).

used in this work was performed on a personal computer with the following configuration: NVIDIA™ GeForce™ GTX 1650 Max Q GPU with 4GB RAM. Once the network is trained, the time required to make predictions is quite short. During the test phase with the data from 2018, the time necessary to open the images and complete the whole processing was around 1 minute (Table 10).

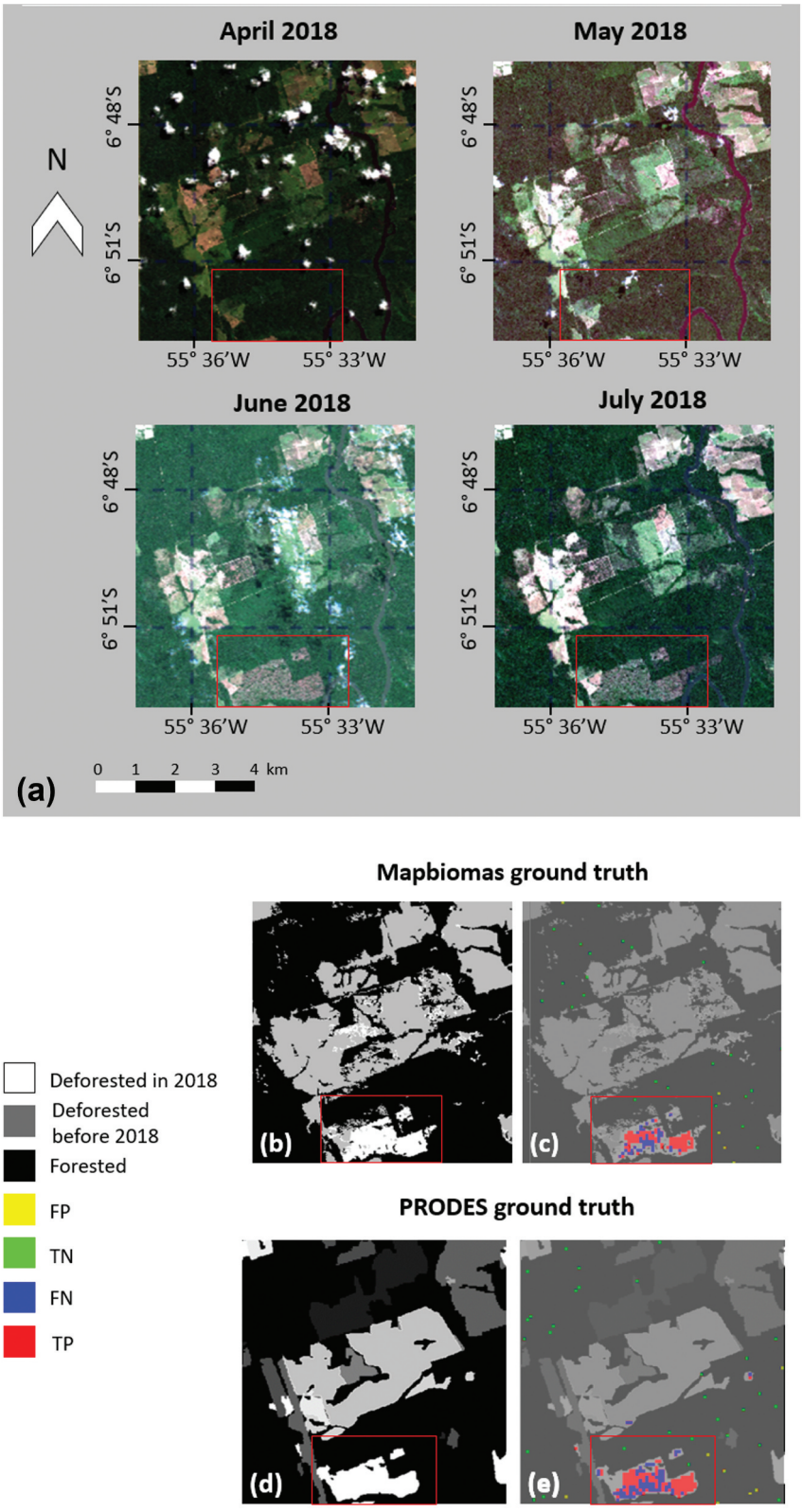

Figure 17. Third example of an area with deforestation (highlighted in red), shown by the Sentinel-2 RGB color composite acquired on April, May, June, and July 2018 (a). MapBiomas ground truth (b), classification output with MapBiomas ground truth (c), PRODES ground truth (d), and classification output with PRODES ground truth (e). FP = False positives (number of forested areas classified as deforested), TN = True negatives (number of forested areas classified as forested), FN = False negatives (number of deforested areas classified as forested), and TP =True positives (number of deforested areas classified as deforested).

Further research should involve strategies to detect deforested areas smaller than 2 ha and use the algorithm as an alert system essential for deforestations related to illegal mining activities in the Brazilian Amazon. In addition, the algorithm could be refined to detect recently deforested areas (slashed areas) and to disregard areas under vegetation regrowth. In this latter case, vegetation

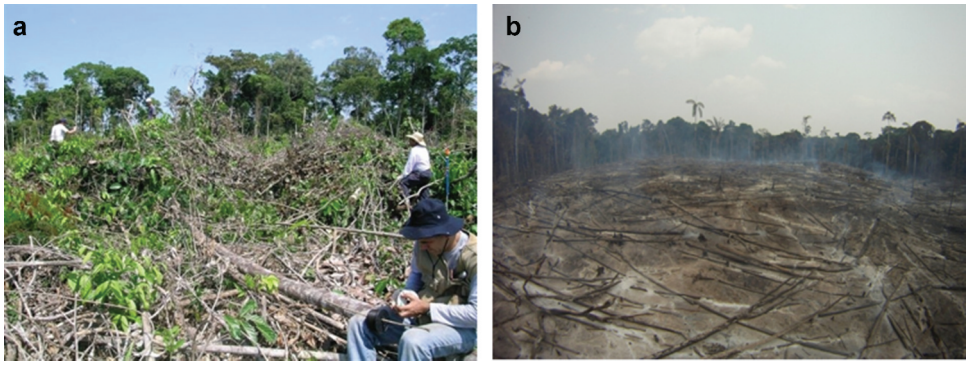

Figure 18. Illustration of a Brazilian Amazon characteristic slashed area (a; Soares Neto et al., 2009) and torched biomass after a fire (b; Christian et al., 2007) found in the Brazilian Amazon.

Table 10. Processing time required during the test phase (2018 data set).

Case study	Processing time (seconds)
1	46.3
2	55.0
3	44.0
4	65.2

indices proposed in literature such as the Normalized Difference Vegetation Index (NDVI), Enhanced Vegetation Index (EVI), or Normalized Difference Water Index (NDWI) can be used to identify the plant growth status and correlate it with forest regrowth (Silva et al., 2019). The method proposed in this study could also be integrated with textural analysis, which exploits correlation among neighbouring pixels, such as those based on the computation of the Gray-Level Co-Occurrence Matrix (GLCM; Del Frate et al., 2008) or geostatistical measures of spatial variability, as suggested by Zawadzki et al. (2005).

Conclusions

In this work, we investigate deforestation in the Amazon rainforest using Sentinel-1 data, and three statistical parameters related to the backscatter coefficient were analysed (mean, standard deviation, and MMD (maximum-minimum difference)). It was observed a backscatter decrease in the average signal of C-band SAR images, approximately 2 dB for VV polarization and 2.3 dB for VH polarization, immediately after deforestation. The decrease is evident for approximately 3–4 months after the deforestation.

The MLP (Multi-Layer Perceptron) was used to detect near real-time forest disturbances larger than 2 hectares. The algorithm analysed SAR images from 2019 for training and 2018 to identify deforest areas automatically. A set of data from 2019 were used to test the performance of the NN (Neural networks) algorithm. Considering the mean, standard deviation, and MMD of the backscatter coefficient as input parameters, the NN was able to classify forested and deforested areas with accuracy and F1 score of 99% for the 2019 data set. For the 2018 data set, the results showed accuracy and F1 score of 89% with MapBiomas ground truth and accuracy and F1 score of 81% and 79%, respectively, with the PRODES ground truth.

The proposed method may be suitable for monitoring forest events in the Amazon at low cost and short processing times and for assisting Brazilian environmental law enforcement agencies in combating illegal deforestation.

Disclosure statement

No potential conflict of interest was reported by the author(s).

Funding

This study was financed in part by the Coordenação de Aperfeiçoamento de Pessoal de Nível Superior, Brasil (CAPES), Finance Code 001, and the National Council for Scientific and Technological Development (CNPq).

Data availability statement

These data were derived from the following resources available in the public domain: [Copernicus at https://scihub.copernicus.eu/]; [MapBiomas Brasil at https://mapbiomas.org/en]; [Terrabrasilis at http://terrabrasilis.dpi.inpe.br/en/home-page/]

References

ALOS Global Digital Surface Model '*ALOS World 3D - 30m' (AW3D30).*" n.d. Jaxa.Jp. https://www.eorc.jaxa.jp/ALOS/en/aw3d30/index.htm. Accessed July 7, 2021

Bem, P., Carvalho Júnior, O., Guimarães, R. F., & Gomes, R. T. (2020). Change detection of deforestation in the Brazilian amazon using Landsat data and convolutional neural networks. *Remote Sensing*, *12*(6), 901. https://doi.org/10.3390/rs12060901

Benediktsson, J. A., Swain, P. H., & Ersoy, O. K. (1990). Neural Network Approaches versus Statistical Methods in Classification of Multisource Remote

Sensing Data. *IEEE Transactions on Geoscience and Remote Sensing*, *28*(4), 540–552. https://doi.org/10.1109/TGRS.1990.572944

Bezerra, T. G., Ruschel, A. R., Emmert, F., & Nascimento, R. G. M. (2021). Changes caused by forest logging in structure and floristic diversity of natural regeneration: Relationship between climate variables and forest dynamics in the Eastern Amazon. *Forest Ecology and Management*, *482*, 118862. https://doi.org/10.1016/j.foreco.2020.118862

Bouguettaya, A., Kechıda, A., & Taberkıt, A. M. (2019). A survey on lightweight CNN-based object detection algorithms for platforms with limited computational resources. *International Journal of Informatics and Applied Mathematics*, *2*(2), 28–44. https://dergipark.org.tr/en/pub/ijiam/issue/52418/654318

Bouvet, A., Mermoz, S., Ballère, M., Koleck, T., & Le Toan, T. (2018). Use of the SAR shadowing effect for deforestation detection with sentinel-1 time series. *Remote Sensing*, *10*(8), 1250. https://doi.org/10.3390/rs10081250

Christian, T. J., Yokelson, R. J., Carvalho Jr, J. A., Griffith, D. W. T., Alvarado, E. C., Santos, J. C., Soares Neto, T. G., Veras, C. A. G., & Hao, W. M. (2007). the tropical forest and fire emissions experiment: Trace gases emitted by smoldering logs and dung from deforestation and pasture fires in Brazil. *Journal of Geophysical Research*, *112*(D18), D18308. https://doi.org/10.1029/2006JD008147

Cochrane, M. A. (2003). Fire science for rainforests. *Nature*, *421*(6926), 913–919. https://doi.org/10.1038/nature01437

Davidson, E. A., Araújo, A. C., Artaxo, P., Balch, J. K., Brown, I. F., Bustamante, M. M. C., Coe, M. T., DeFries, R. S., Keller, M., Longo, M., Munger, J. W., Schroeder, W., Soares-Filho, B. S., Souza, C. M., & Wofsy, S. C. (2012). The Amazon Basin in Transition. *Nature*, *481*(7381), 321–328. https://doi.org/10.1038/nature10717

Davis, K. F., Koo, H. I., Dell'Angelo, J., D'Odorico, P., Estes, L., Kehoe, L. J., Kharratzadeh, M., Kuemmerle, T., Machava, D., Pais, A. D. J. R., Ribeiro, N., Rulli, M. C., & Tatlhego, M. (2020). Tropical forest loss enhanced by large-scale land acquisitions. *Nature Geoscience*, *13*(7), 482–488. https://doi.org/10.1038/s41561-020-0592-3

Del Frate, F., Pacifici, F., & Solimini, D. (2008). Monitoring urban land cover in Rome, Italy, and its changes by single-polarization multitemporal SAR images. *IEEE Journal of Selected Topics in Applied Earth Observations and Remote Sensing*, *1*(2), 87–97. https://doi.org/10.1109/JSTARS.2008.2002221

Del Frate, F., Schiavon, G., Solimini, D., Borgeaud, M., Hoekman, D. H., & Vissers, M. A. M. (2003). Crop classification using multiconfiguration C-Band SAR Data. *IEEE Transactions on Geoscience and Remote Sensing*, *41*(7), 1611–1619. https://doi.org/10.1109/TGRS.2003.813530

Del Frate, F., & Solimini, D. (2004). On neural network algorithms for retrieving forest biomass from SAR data. *IEEE Transactions on Geoscience and Remote Sensing*, *42*(1), 24–34. https://doi.org/10.1109/TGRS.2003.817220

Del Frate, F., & Wang, L.-F. (2001). Sunflower biomass estimation using a scattering model and a neural network algorithm. *International Journal of Remote Sensing*, *22*(7), 1235–1244. https://doi.org/10.1080/01431160151144323

Diniz, C. G., Souza, A. A. A., Santos, D. C., Dias, M. C., Luz, N. C., Moraes, D. R. V., Maia, J. S., Gomes, A. R., Narvaes, I. D. S., Valeriano, D. M., Maurano, L. E. P., & Adami, M. (2015). DETER-B: The new amazon near real-time deforestation detection system. *IEEE Journal of Selected Topics in Applied Earth Observations and Remote Sensing*, *8*(7), 3619–3628. https://doi.org/10.1109/JSTARS.2015.2437075

Doblas, J., Shimabukuro, Y., Sant'Anna, S., Carneiro, A., Aragão, L., & Almeida, C. (2020). Optimizing near real-time detection of deforestation on tropical rainforests using sentinel-1 data. *Remote Sensing*, *12*(23), 3922. https://doi.org/10.3390/rs12233922

Farias, M. H. C. S., Beltrão, N. E. S., Cordeiro, Y. E. M., & Santos, C. A. (2018). Impact of rural settlements on the deforestation of the amazon. *Mercator*, *17*(5), 1–20. https://doi.org/10.4215/rm2018.e17009

Haykin, S. (2009). *Neural Networks and Learning Machines*. Prentice Hall.

Hoekman, D., Kooij, B., Quiñones, M., Vellekoop, S., Carolita, I., Budhiman, S., Arief, R., & Roswintiarti, O. (2020). Wide-area near-real-time monitoring of tropical forest degradation and deforestation using Sentinel-1. *Remote Sensing*, *12*(19), 3263. https://doi.org/10.3390/rs12193263

Joshi, N., Mitchard, E. T. A., Woo, N., Torres, J., Moll-Rocek, J., Ehammer, A., Collins, M., Jepsen, M. R., & Fensholt, R. (2015). Mapping Dynamics of Deforestation and Forest Degradation in Tropical Forests Using Radar Satellite Data. *Environmental Research Letters*, *10*(3), 034014. https://doi.org/10.1088/1748-9326/10/3/034014

Kastens, J. H., Brown, J. C., Coutinho, A. C., Bishop, C. R., Esquerdo, J. C. D. M., & Vadrevu, K. P. (2017). Soy moratorium impacts on soybean and deforestation dynamics in Mato Grosso, Brazil. *PloS One*, *12*(4), e0176168. https://doi.org/10.1371/journal.pone.0176168

Kellndorfer, J. (2019). Using SAR data for mapping deforestation and forest degradation. In A.I. Flores-Anderson, K.E. Herndon, R.B. Thapa, & E. Cherrington (Eds.), *The Synthetic Aperture Radar (SAR) Handbook: Comprehensive Methodologies for Forest Monitoring and Biomass Estimation* (pp. 65–79). SERVIR Global Science Coordination Office, National Space Science and Technology Center.

Laurin, G. V., Avezzano, R., Bacciu, V., Del Frate, F., Papale, D., & Virelli, M. (2018). COSMO-skymed potential to detect and monitor Mediterranean maquis fires and regrowth: A pilot study in capo Figari, Sardinia, Italy. *IForest: Biogeosciences and Forestry*, *11*(3), 389–395. https://doi.org/10.3832/ifor2623-011

Laurin, G. V., Liesenberg, V., Chen, Q., Guerriero, L., Del Frate, F., Bartolini, A., Coomes, D., Wilebore, B., Lindsell, J., & Valentini, R. (2013). Optical and SAR sensor synergies for forest and land cover mapping in a tropical Site in West Africa. *ITC Journal*, *21*, 7–16. http://dx.doi.org/10.1016/j.jag.2012.08.002

"Mapbiomas Brasil." n.d. *Mapbiomas.Org*. https://mapbiomas.org/en. Accessed July 7, 2021

Matricardi, E. A. T., Skole, D. L., Costa, O. B., Pedlowski, M. A., Samek, J. H., & Miguel, E. P. (2020). Long-term forest degradation surpasses deforestation in the Brazilian Amazon. *Science*, *369*(6509), 1378–1382. https://doi.org/10.1126/science.abb3021

Nepstad, D., Carvalho, G., Barros, A. C., Alencar, A., Capobianco, J. P., Bishop, J., Moutinho, P., Lefebvre, P., Silva, U. L., Jr., & Prins, E. (2001). Road paving, fire regime feedbacks, and the future of amazon forests. *Forest Ecology and Management*, *154*(3), 395–407. https://doi.org/10.1016/S0378-1127(01)00511-4

Nepstad, D. C., Verssimo, A., Alencar, A., Nobre, C., Lima, E., Lefebvre, P., Schlesinger, P., Potter, C., Moutinho, P., Mendoza, E., Cochrane, M., & Brooks, V. (1999). Large-scale impoverishment of Amazonian forests by logging and fire. *Nature*, *398*(6727), 505–508. https://doi.org/10.1038/19066

Open Access Hub. n.d. *Copernicus.Eu*. Accessed July 7, 2021. https://scihub.copernicus.eu/

Potin, P., Rosich, B., Miranda, N., Grimont, P., Shurmer, I., O'Connell, A., Krassenburg, M., & Gratadour, J.-B. 2019. "Copernicus Sentinel-1 constellation mission operations status." In *Proceedings of the 2019 IEEE International Geoscience and Remote Sensing Symposium (IGARSS 2019)*, Yokohama, Japan. http://dx.doi.org/10.1109/igarss.2019.8898949

Pratola, C., Del Frate, F., Schiavon, G., & Solimini, D. (2013). Toward fully automatic detection of changes in suburban areas from VHR SAR images by combining multiple neural-network models. *IEEE Transactions on Geoscience and Remote Sensing*, *51*(4), 2055–2066. https://doi.org/10.1109/TGRS.2012.2236846

Prechelt, L. (1998). Early stopping - but when? In *Lecture Notes in Computer Science* (pp. 55–69). Springer, Berlin, Heidelberg. http://dx.doi.org/10.1007/3-540-49430-8_3

Ramchoun, H., Amine, M., Idrissi, J., Ghanou, Y., & Ettaouil, M. (2016). Multilayer perceptron: Architecture optimization and training. *International Journal of Interactive Multimedia and Artificial Intelligence*, *4*(1), 26–30. https://doi.org/10.9781/ijimai.2016.415

Reiche, J., Hamunyela, E., Verbesselt, J., Hoekman, D., & Herold, M. (2018a). Improving near-real time deforestation monitoring in tropical dry forests by combining dense sentinel-1 time series with Landsat and ALOS-2 PALSAR-2. *Remote Sensing of Environment*, *204*, 147–161. https://doi.org/10.1016/j.rse.2017.10.034

Reiche, J., Verbesselt, J., Hoekman, D., & Herold, M. (2015). Fusing Landsat and SAR time series to detect deforestation in the tropics. *Remote Sensing of Environment*, *156*, 276–293. https://doi.org/10.1016/j.rse.2014.10.001

Reiche, J., Verhoeven, R., Verbesselt, J., Hamunyela, E., Wielaard, N., & Herold, M. (2018b). Characterizing tropical forest cover loss using dense sentinel-1 data and active fire alerts. *Remote Sensing*, *10*(5), 777. https://doi.org/10.3390/rs10050777

Sharma, S., Sharma, S., & Athaiya, A. (2020). Activation functions in neural networks. *International Journal of Engineering Applied Sciences and Technology*, *4*(12), 310–316. https://doi.org/10.33564/IJEAST.2020.v04i12.054

Silva, C. A., Santilli, G., Sano, E. E., & Laneve, G. (2021). Fire occurrences and greenhouse gas emissions from deforestation in the Brazilian Amazon. *Remote Sensing*, *13*(3), 376. https://doi.org/10.3390/rs13030376

Silva, C. A., Santilli, G., Sano, E. E., & Rodrigues, S. W. P. (2019). Análise qualitativa do desmatamento na Floresta Amazônica a partir de sensores SAR, óptico e termal. *Anuário Do Instituto de Geociências*, *42*(4), 18–29. https://doi.org/10.11137/2019_4_18_29

Silva Júnior, C., Aragão, L., Fonseca, M., Almeida, C., Vedovato, L., & Anderson, L. (2018). Deforestation-induced fragmentation increases forest fire occurrence in central Brazilian Amazonia. *Forests*, *9*(6), 305. https://doi.org/10.3390/f9060305

SNAP Download. n.d. *Esa.Int*. https://step.esa.int/main/download/snap-download/. Accessed July 7, 2021

Soares Neto, T. G., Carvalho Jr, J. A., Veras, C. A. G., Alvarado, E. C., Gielow, R., Lincoln, E. N., Christian, T. J., Yokelson, R. J., & Santos, J. C. (2009). Biomass Consumption and CO_2, CO and main hydrocarbon gas emissions in an Amazonian forest clearing fire. *Atmospheric Environment*, *43*(2), 438–446. https://doi.org/10.1016/j.atmosenv.2008.07.063

Souza, C. M., Jr., Shimbo, J. Z., Rosa, M. R., Parente, L. L., Alencar, A. A., Rudorff, B. F. T., Hasenack, H., Matsumoto, M., G. Ferreira, L., Souza-Filho, P. W. M., de Oliveira, S. W., Rocha, W. F., Fonseca, A. V., Marques, C. B., Diniz, C. G., Costa, D., Monteiro, D., Rosa, E. R., Vélez-Martin, E., … Azevedo, T. (2020). Reconstructing three decades of land use and land cover changes in Brazilian biomes with Landsat archive and earth engine. *Remote Sensing*, *12*(17), 2735. https://doi.org/10.3390/rs12172735

Stramondo, S., Del Frate, F., Picchiani, M., & Schiavon, G. (2011). Seismic source quantitative parameters retrieval from insar data and neural networks. *IEEE Transactions on Geoscience and Remote Sensing*, *49*(1), 96–104. https://doi.org/10.1109/TGRS.2010.2050776

"Terrabrasilis – Geographic Data Platform." n.d. *Inpe.Br*. http://terrabrasilis.dpi.inpe.br/en/home-page/. Accessed July 7, 2021

Torres, R., Snoeij, P., Geudtner, D., Bibby, D., Davidson, M., Attema, E., Potin, P., Rommen, B., Floury, N., Brown, M., Traver, I. N., Deghaye, P., Duesmann, B., Rosich, B., Miranda, N., Bruno, C., L'Abbate, M., Croci, R., Pietropaolo, A., … Rostan, F. (2012). GMES Sentinel-1 Mission. *Remote Sensing of Environment*, *120*, 9–24. https://doi.org/10.1016/j.rse.2011.05.028

van Marle, M. J. E., Field, R. D., van der Werf, G. R., Wagt, I. A. E., Houghton, R. A., Rizzo, L. V., Artaxo, P., & Tsigaridis, K. (2017). Fire and deforestation dynamics in Amazonia (1973–2014). *Global Biogeochemical Cycles*, *31*(1), 24–38. https://doi.org/10.1002/2016GB005445

Yanai, A. M., Graça, P. M. L. A., Escada, M. I. S., Ziccardi, L. G., & Fearnside, P. M. (2020). Deforestation dynamics in Brazil's Amazonian Settlements: Effects of land-tenure concentration. *Journal of Environmental Management*, *268*(110555), 110555. https://doi.org/10.1016/j.jenvman.2020.110555

Yanai, A. M., Nogueira, E. M., Graça, P. M. L. A., & Fearnside, P. M. (2017). Deforestation and carbon stock loss in Brazil's Amazonian settlements. *Environmental Management*, *59*(3), 393–409. https://doi.org/10.1007/s00267-016-0783-2

Zawadzki, J., Cieszewski, C. J., Zasada, M., & Lowe, R. C. (2005). Applying geostatistics for investigations of forest ecosystems using remote sensing imagery. *Silva Fennica*, *39*(4), 599–617. https://doi.org/10.14214/sf.369

Copernicus Sentinel data (2021), processed by ESA. https://scihub.copernicus.eu/